Development of new artificial biomembrane systems and their characterization based on mesoscopic morphology and lateral diffusion

（新規人工生体膜系の開発およびメソスケール領域における構造と側方拡散性に基づいた特性評価）

January, 2017

Doctor of Engineering

Yoshiaki Okamoto

岡本　吉晃

Toyohashi University of Technology

Index

Chapter 1

Introduction

Chapter 1. Introduction

1-1. Importance and history of biomembrane studies

Cells are the smallest unit of the structure and function of all living matters, isolated from outer environment by thin membrane called plasma membrane. In the cells subcellular organelles exist such as cell nucleus, Golgi body, and mitochondria, which are also configured by thin membranes. These membrane-like structures are collectively called biomembranes, and have common fundamental structure of bimolecular layer. If we focus on plasma membranes, they behave as not only the partition to separate cells from external environments, but also the reaction field for various membrane reactions: transport of materials into and out of cells, sending and receiving of information, and discharging of the metabolites. The functions of the plasma membranes deeply relate their fundamental structure, a bimolecular layer of lipid molecules (Figure 1-1).

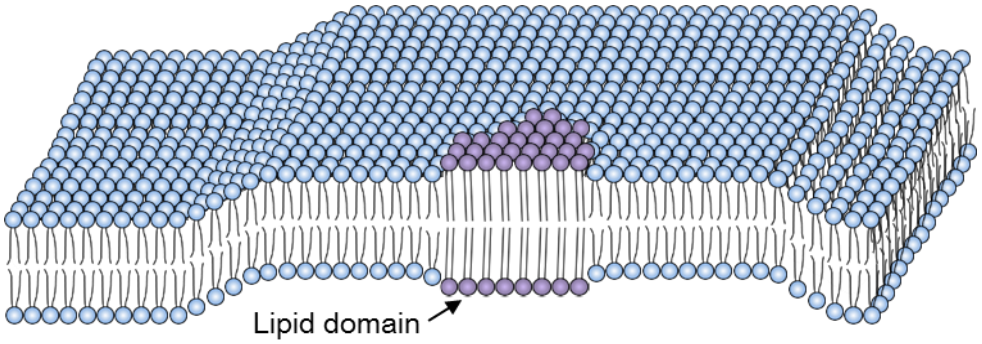

Figure 1-1. Schematic image of lipid bilayer.

In 1925, E. Gorter and F. Grendel first proposed that biomembranes are composed of a bimolecular layer structure of lipid molecules.[1)] They prepared a monolayer film by diffusing lipids extracted from a red blood cell onto a water surface. Because the area of obtained lipid monolayer was twice the total surface area of the original red blood cells, they got an idea that

the membrane of red blood cells was composed of bimolecular structure of lipids. Since their discovery, the concept of lipid bilayer has been established.

In 1935, H. Davson and J. Danielli proposed the first biomembrane model including membrane proteins that biomembranes are lipid bilayer covered with proteins.[2] This biomembrane model was supported for about 30 years, because this model was correct for thermodynamically stable that amphiphilic lipids form the bilayer structure, although proteins state was incorrect.

In 1964, A. D. Bangham and R. W. Horne reported that multilamellar vesicle was formed spontaneously by suspending phosphatidylcholines, which are amphiphilic phospholipid and derived from chicken egg, into water.[3] Phospholipids are amphiphilic molecules with a hydrophilic head group and hydrophobic chains. In aqueous solutions they assemble spontaneously the lipid bilayer keeping their hydrophobic chains inside, and facing the hydrophilic head groups to water.

In the previous conventional biomembrane model, biological membranes were considered to be a static structure. Since 1970, however, the interest in a fluidity of lipid bilayer increased. It had been revealed that lipid molecules are able to diffuse in lipid bilayer freely. A lipid bilayer structure stably exists because of hydrophilic and hydrophobic interaction, but if we see the interaction inside the bilayer, major inter-molecular interaction is van der Waals' force and strong interaction like a covalent bond does not exist among lipid molecules. Therefore, each lipid molecules are able to diffuse laterally in lipid bilayer without jumping out of lipid bilayer by thermal diffusion.

On the basis of various findings including those mentioned above, S. J. Singer and Garth L. Nicolson proposed the fluid mosaic model in 1972.[4] According to this model, biomembranes are a fluid lipid bilayer containing proteins embedded in a mosaic pattern. The fluid mosaic

model is superior in explaining the concept of the membrane fluidity, unlike conventional models that separate lipids and proteins. Therefore, this model was widely accepted and became the basis of posterity biomembrane studies.

The fundamental structure of biomembranes is a lipid bilayer, but actually biomembranes are composed of various kinds of biomolecules including phospholipids, cholesterol, glycolipids, proteins, etc. The composition of lipids varies significantly depending on species and tissues. Following the fluid mosaic model, we should obtain the membrane fluidity as the average value of molecule motion in the membrane. Recent development of microscopic technology allowed us the observation of single molecule diffusing in a local space, and it is becoming clear that biomembranes are not homogeneous mixtures of lipids and proteins. The fluidity of biomembrane is controlled by the lipid composition and the diffusion barrier caused by membrane proteins. Therefore it is expected that the reaction rate and efficiency is increased by enclosing the required membrane proteins.

K. Simons proposed that two-dimensional domains consisting of specific lipids, such as sphingolipids and cholesterol, and specific proteins crucial for signal transportation are formed in biomembranes, and such domains are called “lipid raft”.[5] This lipid domain play roles in folding the membrane proteins into collect form, and concentrating the proteins and lipids necessary for the signalization and the transport of materials via endocytosis and exocytosis. Formation of lipid domains occurs spontaneously also in artificial lipid bilayer systems containing several kinds of lipids (Figure 1-1).

Lipid composition of biomembrane in living cell is different between the inner leaflet and the outer leaflet. In the human red blood cell membrane, for example, the most of negatively-charged lipids exist in the inner leaflet, and all lipid molecules with saccharide chain are existed in outer leaflet. This asymmetric distribution of lipid bilayers is important for

transducing the signal from outside of cell to inside. The lipid composition of inner leaflet and that of outer leaflet is rarely changed, because the diffusion of lipids between the inner leaflet and the outer leaflet, that is called flip-flop, is very slowly. When newly produced lipids are supplied to biomembrane, the proteins controlling the flip-flop such as flippase and floppase maintain the asymmetry of lipid bilayer. The asymmetry of lipid composition and the orientation of proteins are essential properties for the directional matter transport into and out of cell.

The fluidity and the asymmetry of lipid bilayer play important roles for membrane reactions in considering the various functions of membrane protein. Dysfunction of membrane proteins and anomalous membrane reactions are deeply involved with serious diseases such as central neurological diseases and metabolic disorders.[6] In a recent review, it was reported that 60% of all presently known over 430 drug targets are membrane proteins.[7] Therefore, the elucidation of the mechanism of membrane reactions including the structure and function of membrane proteins and the physicochemical property of lipid bilayer is also highly significance in the drug discovery and medical fields.

1-2. Artificial lipid membranes

Plasma membrane is intricate system consisting of various factors. To understand the elementary steps of membrane reactions occurred in biomembrane, understanding of the nature of lipids and lipid bilayers is needed. Usage of artificial lipid bilayers is a straightforward and effective strategy for this purpose. Therefore, several kinds of artificial lipid bilayer systems have been developed as model systems of plasma membranes. Since the discovery by Bangham in 1964 that lipid bilayer is formed spontaneously by stirring the lipid molecules into aqueous solution,[3] lipid vesicles which are the spherical shell structure made of lipid bilayer, have been

investigated as a representative plasma membrane model extensively. Other artificial lipid bilayer systems with a planar structure as typified by the black lipid membrane (BLM) and the supported lipid bilayer (SLB) have been also used for the investigation of the physicochemical properties of lipid bilayers and the functions and structure of membrane proteins.

Vesicles are spherical structures of lipid bilayer, and are used extensively as the cell-membrane model from because of their similarity in the closed-shell structure to cells. A suspension of vesicles is prepared by dispersing lipid molecules into an aqueous solution. Several methods are established to control the size and lipid composition of vesicle by the procedures of sonication and extrusion with a microporous film. Vesicles are also used for the isolation and purification of the membrane proteins, because membrane-spanning and membrane-embedded proteins are denatured easily by exposing their hydrophobic parts to water or organic solvents.

BLM is an artificial planar membrane formed across a 1 nm hole between two solution chambers, and is named from the appearance by optical microscope. Solution of lipid in an organic solvent is painted at a hole on a hydrophobic sheet, monolayers of lipids form at the both interfaces between the organic solvent and the aqueous solutions of the two chambers and monolayers finally binds up to a single lipid bilayer. In the 1960s, Mueller and coworkers developed the first BLM system for the investigation of the electrical properties of a planar lipid bilayer such as the permeability, membrane current, and membrane potential.[8,9] BLM systems are also used as the platform to investigate the electrical properties of transmembrane-type proteins such as ion channels. Although generally it is not possible to insert membrane proteins in lipid membrane directly because of denaturing the membrane proteins in an organic solvent, we are able to reconstruct membrane proteins by the solubilization of membrane proteins using surfactant, or the addition of proteoliposome containing membrane proteins. In BLMs the transmembrane proteins suspended within the lipid bilayer remain fully mobile and active

because BLMs are suspended in solution without a support to the solid substrate. This flexibility also leads to fragility of membrane, therefore the lifetime of BLMs is limited. There is also the effect of the residual organic solvent on the membrane proteins reconstructed in the lipid bilayer.[10)]

SLB is an artificial lipid bilayer formed at the interface between an aqueous solution and a hydrophilic solid substrate. Because the SLB systems are more stable and robust than the free-standing membrane systems such as the vesicles and BLM above, we can measure the physicochemical properties using the surface analytical techniques which are not available for the vesicle and BLM systems. In SLB systems the fluidity of the lipid membrane is maintained by the approximately 1 nm thick water layer between the lipid bilayer and the substrate surface.[11)] Therefore, SLB is used as a cell-membrane model for the investigation of the phenomenon with the dynamic process of the lipid bilayer such as the molecular diffusion and the organization of two-dimensional domains using the high resolution and high sensitivity surface scientific techniques as represented by the scanning probe microscopy. Furthermore, SLBs are exploited for the nanotechnology. In 1997 S. G. Boxer and coworkers have succeeded in area-selective forming the SLBs by patterning the substrate using lithographic techniques.[12)] This has led to the development of individually addressed arrays of SLBs by P. S. Cremer and T. Yang[13)] and sensor arrays for the study of cell adhesion by J. T. Groves and coworkers.[14)] These SLB assays combined with microfluidic systems are also applied as a powerful sensor such as the immunoassays to study the antigen-antibody reaction on the lipid bilayer.

For the formation of the SLB systems, there are mainly three methods: the Langmuir-Blodgett/Schaefer method, the vesicle fusion method, and the self-spreading method.

The Langmuir-Blodgett/Schaefer method is the first method to fabricate the bilayer structure of amphiphilic molecules.[15)] Amphiphilic molecules which are floated at the air-water interface are

arranged regularly and formed a monolayer by the lateral compression. It is called Langmuir film. The Langmuir monolayer, at the air-water interface is carried to a solid substrate which is pulled up from the aqueous solution to air through the monolayer. If the substrate with the monolayer is sequentially pushed back to the aqueous solution covered with the Langmuir monolayer on its surface horizontally, another monolayer deposited and a bimolecular layer is formed. It is called Langmuir-Blodgett method. There is the other method for carrying the second Langmuir monolayer onto the first Langmuir monolayer on a solid substrate by placing the substrate parallel to the water surface in contact with the Langmuir monolayer. It is called Langmuir-Schaefer method.[16)] One can prepare SLBs by carrying out the Langmuir-Blodgett/Schaefer method using lipids.[17–23)] The Langmuir-Blodgett and Langmuir-Schaefer techniques are available for various kinds and components lipid molecules, but a matured technical skill is needed to prepare the SLB reproducibly.

The vesicle fusion method is another method for the formation of SLBs with a simple operation of immersion of a hydrophilic substrate into a vesicle suspension.[6,12,13,24–53)] In the vesicle fusion method, SLB is formed spontaneously through the processes of the adsorption of vesicles to substrate surface and the subsequent fusion and/or rupture of adsorbed vesicles. For the transform from a vesicle to a planar lipid membrane, it is necessary to keep the temperature higher than the transition temperature between the gel and liquid crystalline phases of the lipid membrane. The advantage of this method is that it is possible to form a homogeneous SLB regardless of the shape and size of the substrate. However, it is known that in vesicle fusion method the conditions during the incubation such as the composition of lipid vesicles, the size of vesicles, the ion concentration in the aqueous solution, and the nature of substrate affects the transformation process to the planar membranes. In some cases a stabilized adsorbed vesicle layer is formed depending on the conditions. Factors affecting the formation of SLB on

substrate surfaces are for example the materials, concentration of chemical functional groups, and electro-static change density on the surfaces. On a hydrophilic surface, vesicles change the shape to the planar membrane keeping the bilayer structure. On the other hand, on a hydrophobic surface, for example covered with the self-assembled monolayer (SAM) of hydrocarbon chains, the monolayer of lipid is formed on SAM by the disassociation of associating hydrocarbon chains is opened.[26,29] This technique enables to place the SLB and the hybridized lipid monolayer/SAM by the patterning of SAM.[34]

When a substrate which is attached with a chunk of lipid molecules is immersed into an aqueous solution, self-assembled lipid bilayers grow and spread along the substrate surface from the foot of the lipid chunk. This phenomenon is called self-spreading, and applied to the formation of SLB.[54–61] A unique characteristic of the self-spreading method is the sequential formation of SLB by the supply from the lipid source. Using this characteristic, it is possible to develop a system similar to microfluidic devices by controlling the direction and position of self-spreading through the patterning of the substrate surface. The advantage of the self-spreading is the application for novel devices such as molecular separation and molecular gate devices[61]. On the other hand, the self-spreading method is not suitable for the fabrication of a large-are SLB in a short period of time.

1-3. Graphene oxide and its biological application

Graphene oxide (GO) is one of the graphene-based carbon materials, and is exploited for the biological application using specific properties originated from the graphene structure (Figure 1-2). Graphene is a single-atom-thick planar sheet of carbon atoms densely packed in a honeycomb crystal lattice. Graphene attracts great interests in the field of electrical engineering,

electronics, and semiconductor derived because of its excellent electrical, physical, and chemical properties.[62–73)]

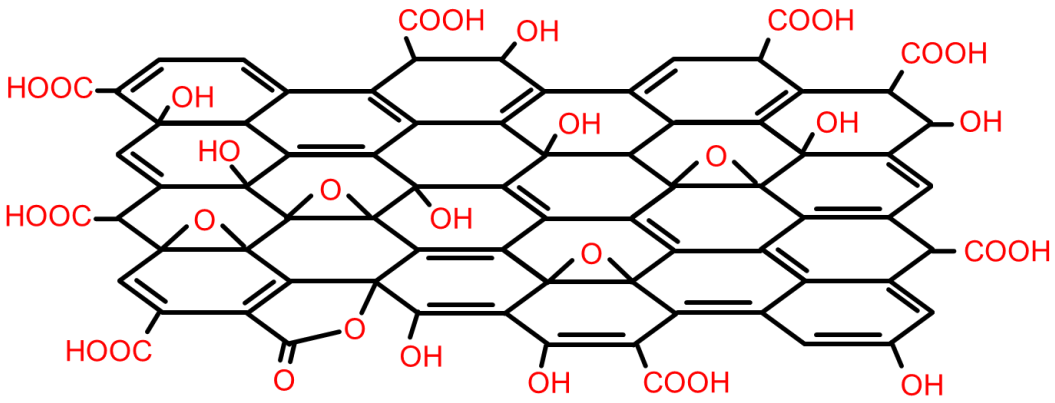

Figure 1-2. Schematic image of graphene oxide.

Previously, graphene was treated as a theoretical model for the investigation of several carbon materials such as graphite, fullerene, and carbon nanotube, because the theoretical prediction presumed that graphene would be unstable due to thermal fluctuations. The great accomplishment in the isolation of graphene in atmosphere and the measurement of its property by A. K. Geim and K. S. Novoselov was awarded the Nobel Prize in Physics in 2010. In 2004 they first reported the success in the isolation of a graphene sheet by the mechanical exfoliation of the highly oriented pyrolytic graphite using the adhesive tape, and in the measurement of the electric properties of the obtained graphene.[62)] Graphene exhibits a lot of excellent physical and electrical properties such as the high electrical and thermal conductivity, the high carrier mobility, the mechanical strength, and the quantum Hall effect at room temperature, and is expected as the next-generation material to exploit for single-electron transistors, flexible displays, and solar cells. After the report of the isolation of graphene from graphite by A. K. Geim and K. S. Novoselov, various methods for the fabrication of graphene have been reported. Representatives are the mechanical cleavage the epitaxial growth, the chemical vaper deposition

(CVD), and the chemical synthesis had been developed.[68,69,74)]

Mechanical cleavage is the simplest method to isolate the near perfect graphene from graphite flakes by peeling repeatedly using an adhesive tape without the expensive instruments. A pristine graphene sheet obtained by this method is useful for fundamental studies to characterize the physical, electrical and chemical properties. However, this technique is unsuitable for the mass production, and should be noted the glue residues from the tape on substrate surface.

Epitaxial growth is a method to obtain the graphene on the single-crystal silicon carbide substrate by the sublimation of silicon atoms and the reorganization of carbon atoms through the thermal treatment of silicon carbide.[75,76)] The major advantage of the epitaxial-grown graphene is that it is capable of patterning by standard lithography techniques. However, it is very hard to isolate the graphene sheet from the silicon carbide substrate.

CVD is a method for the preparation of the thin film by the exposure of substrate to thermally decomposed precursors and the deposition of the desired component product on the substrate surface at high temperature. CVD is widely used for solid film coatings to substrates. In CVD methods, graphene is prepared directly on a transition metal substrate such as copper and nickel by the saturation of carbon upon exposure to a hydrocarbon gas at a high temperature.[77–79)] When the substrate is cooled, the solubility of carbon in the substrate decreases and the carbon precipitates to form monolayer or multilayer graphene sheets on the substrate. The CVD technique has high compatibility with the complementary metal-oxide semiconductor (CMOS) technology. The advantages of CVD method are that the graphene sheet is produced on a large-scale compared with other methods. On the other hand, disadvantages of CVD method are that the control of film thickness is difficult and secondary crystals are easily formed.

Chemical synthesis is a chemical method to obtain graphene by the chemical exfoliation of graphite to prepare graphene oxide (GO) and the subsequent reduction of GO.[80–84)] The

chemical exfoliation involves the synthesis of GO by oxidation of graphite with strong acids and oxidants, and dispersing the oxidized graphite into the solution to isolate single layer GO. It was B. Brodie who first reported in 1895 that a thin layer of carbon sheet was obtained by the oxidation of graphite with nitric and sulfuric acids.[85] This methodology for obtaining "graphite oxide" was improved by W. S. Hummers and co-workers and reported in1958.[86] This method is called Hummers method, and attracted a great deal of attention as a method for preparing after the discovery of graphene: people found that single atomic sheets were also included in the suspension of graphite oxide. Then the obtained GO flake is reduced for the recovery the graphene structure. The electrical and physical properties of reduced GO obtained by this method significantly inferior compared with graphene obtained from other methods because of the structural defect such as the hole and the residual oxidized region. The chemical synthesis of graphene has several advantages such as the low temperature process and the large-scale production at low cost.

Recently, the biological application using graphene derivatives was investigated extensively because the specific ability as the fluorescence quencher resulted from the single atomic layer structure of graphene is attracted the great attention in the field of biological application. In 2009 C. Lu and coworkers reported the detection of the DNA hybridization using the specific fluorescence quenching by GO.[87] GO has a structure consisting of the nanoscale sp^2-carbon region like the graphene within the sp^3-carbon matrix with oxygen functional group such as epoxy, hydroxyl, and carboxyl group (Figure 1-2),[88,89] and also has the specific fluorescence quenching ability originated in the graphene structure.[67,89–91] Unlike graphene, single GO sheet is dispersible stably in water and several organic solvents, because the oxidized hydrophilic region is majority on the GO surface. These oxidized regions are also available for the chemical modification. Therefore, GO is the more biocompatible than pristine graphene, and is

advantageous for the sensing of biological binding reactions such as DNA hybridization,[84,87,92,93] antigen-antibody reaction,[83,89,94] and aptamer binding.[95,96]

1-4. Fluorinated phospholipid

Specific functions appeared by the introduction of fluorine atom to various compounds leads to drastic developments in the various research fields. Fluorine atom has a largest electronegativity among all atoms, and binds with carbon atom strongly. The fluorine-introduced materials exhibit the remarkable properties such as the excellent resistance to heat, light, and chemicals, repellency against water and oil, electrical insulation, and increase in drug efficacy.

The fluorinated lipids and surfactants are expected for the biological application such as the surface modification for the biomimetic materials, drug delivery system, and the extraction of proteins because of the biological inertness due to the weak intramolecular interaction and the chemical stability. Frotscher and coworkers reported that the fluorinated octylmaltoside derivative F_6OM has superior performance compared with a lipophobic fluorinated surfactant in chaperoning the functional refolding of an integral membrane enzyme.[97] This is because its mild and unusual mode of detergency promotes the bilayer insertion.

Recently, Sonoyama and co-workers synthesized a novel partially fluorinated lipid 1,2-di-(11,11,12,12,13,13,14,14,14-nonafluorotetradecanoyl)-sn-glycero-3-phophocholine (F4-DMPC, which was expressed as diF4H10 in the literatures[98–100], an analog of a common 1,2-dimyristoyl-sn-glycero-3-phosphocholine (DMPC) with the perfluorinated butyl segment in the myristoyl group, and investigated its thermal and interfacial properties.[98,99] The results of the differential thermal calorimetry (DSC) measured for the mixture of F4-DMPC and DMPC indicate that the interaction between F4-DMPC and DMPC cannot be simply interpreted only in

terms of the separation between fluorocarbons and hydrocarbons.[98,99] They also revealed that the bacteriorhodopsin reconstructed in the vesicle of F4-DMPC retains the nativelike structure, optical function and stability against visible light even in the liquid crystalline phase.[100] These results strongly suggest that the F4-DMPC affects to lipids and membrane proteins in a different manner from the common phospholipids with hydrocarbon chains.

1-5. Scope and purpose of this thesis

In the above sections, I described the importance of the study of plasma membranes and the effectiveness of the usage of artificial lipid bilayer systems. Also as described above, the biological applications using the specific fluorescence quenching ability of GO and the fluorinated lipid with the specific function derived from a fluorine atom are investigated extensively. In this thesis, I constructed new artificial lipid bilayer systems on the basis of SLB, and revealed its structure and physicochemical properties. I developed the artificial lipid bilayer systems for the measurement of biomolecule behaviors in lipid bilayers, and I evaluated their structures and physicochemical properties based on the mesoscopic morphology and the lateral diffusion.

I expect that the artificial cell membrane system formed on GO leads to a new method to measure the detailed behavior of biomolecules such as lipids, membrane proteins in lipid bilayer with a high degree of accuracy using the unique fluorescence quenching by GO. The fluorescence quenching by graphene and GO is independent of the wavelength of donor fluorescence probe,[66,67,89] and the effective range, which is expressed as the Förster radius, is longer than those of general quencher molecules.[66,101] In the theoretical calculation based on the Förster mechanism, the efficiency of fluorescence quenching by graphene has dependence on

the minus forth power of the distance between a donor fluorophore and graphene,[71,102] while the efficiency of quenching by general quencher molecule is dependence to the minus sixth power of the intermolecular distance.[103–105] GO also exhibits the fluorescence quenching ability similar to graphene. In fact, J. Liu and coworkers demonstrated that the quenching efficiency (E) of GO was expressed as $E = 1/[1+(R/R_0)^4]$, where R is the distance between donor and GO, R_0 is the Förster distance of GO.[102] The concept of the SLB/GO system using the unique fluorescence quenching is shown in Figure 1-3. In the SLB/GO systems, the fluorescence probes labeled to lipids and membrane proteins, which are described as "Fluorophore" in Figure 1-3 are quenched by GO. According to the FRET theory as mentioned above, however, the effective range of the fluorescence quenching by GO is longer than that by general quencher molecules, and the florescence intensities of the fluorophores decreases with the distance from GO. Because the quenching efficiency of GO depends on the minus fourth power of the distance between the fluorophore and GO, a slight difference in the distance between fluorophore and GO affects fluorescence intensity significantly. Therefore, we expect that the SLB/GO system is capable of measuring nanoscale changes in biomembranes such as the transition of lipid bilayer thickness

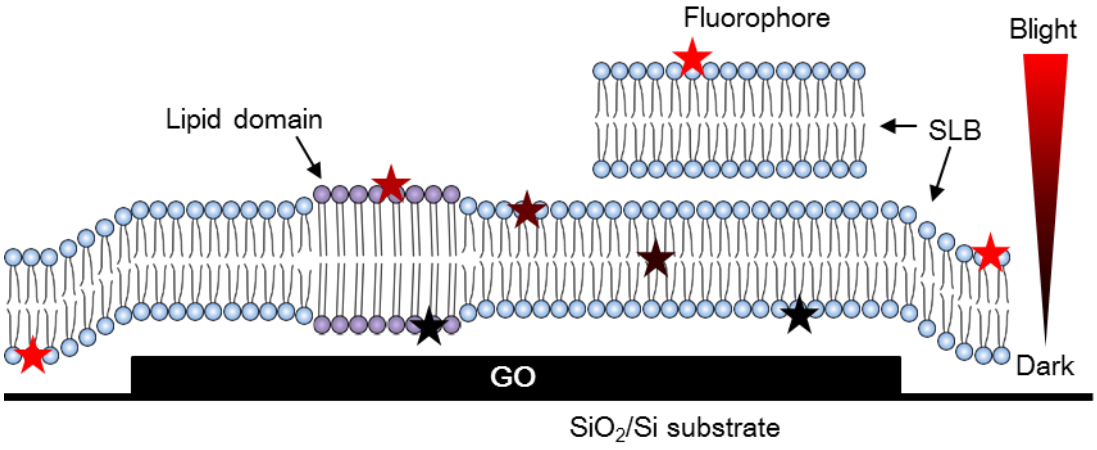

Figure 1-3. Concept of SLB/GO system for the measurement of biomolecule behaviors using the unique fluorescence quenching by GO.

associated with the organization of lipid domains and the conformation change of membrane proteins on the basis of the fluorescence intensity which is dependence on the distance from the GO.

As the first step for the construction of the SLB/GO system, I formed SLB on GO by the vesicle fusion method. It is described in Chapter 3. To evaluate the fluidity of SLB formed on GO, I conjugated quantum dots (Qdots) as a brighter probe than dye-labeled lipids to the SLB surface. It is described in Chapter 4. I measured the fluorescence intensity to evaluate the distance dependency of the quenching efficiency of GO, and evaluated the diffusion coefficient of the SLB formed on GO (Chapter 5). As another subject in this thesis, I investigated the physicochemical properties of F4-DMPC in SLB system in Chapter 6. I evaluated the lateral mobility of F4-DMPC and its temperature dependence as the index to estimate the intermolecular interaction of the partially fluorinated lipid.

Reference

1) E. Gorter and F. Grendel, J. Exp. Med. **41**, 439 (1925).

2) J. F. Danielli and H. Davson, J. Cell. Comp. Physiol. **5**, 495 (1935).

3) A. D. Bangham and R. W. Horne, J. Mol. Biol. **8**, 660 (1964).

4) S. J. Singer and G. L. Nicolson, Science **175**, 720 (1972).

5) D. Lingwood and K. Simons, Science **327**, 46 (2010).

6) R. Tero, H. Watanabe, and T. Urisu, Phys. Chem. Chem. Phys. **8**, 3885 (2006).

7) L. Tiefenauer and S. Demarche, Materials **5**, 2205 (2012).

8) P. Mueller, D. O. Rudin, H. T. Tien, and W. C. Wescott, Nature **194**, 979 (1962).

9) P. Mueller, D. O. Rudin, H. T. Tien, and W. C. Wescott, J. Phys. Chem. **67**, 534 (1963).

10) E. T. Castellana and P. S. Cremer, Surf. Sci. Rep. **61**, 429 (2006).

11) P.-E. Milhiet, F. Gubellini, A. Berquand, P. Dosset, J.-L. Rigaud, C. Le Grimellec, and D. Lévy, Biophys. J. **91**, 3268 (2006).

12) J. T. Groves, N. Ulman, and S. G. Boxer, Science **275**, 651 (1997).

13) P. S. Cremer and T. Yang, J. Am. Chem. Soc. **121**, 8130 (1999).

14) J. T. Groves, L. K. Mahal, and C. R. Bertozzi, Langmuir **17**, 5129 (2001).

15) L. K. Tamm and H. M. McConnell, Biophys. J. **47**, 105 (1985).

16) I. Langmuir and V. J. Schaefer, J. Am. Chem. Soc. **60**, 1351 (1938).

17) J. Zasadzinski, R. Viswanathan, L. Madsen, J. Garnaes, and D. Schwartz, Science **263**, 1726 (1994).

18) T. Schmidt, G. J. Schütz, W. Baumgartner, H. J. Gruber, and H. Schindler, Proc. Natl. Acad. Sci. U. S. A. **93**, 2926 (1996).

19) G. J. Schütz, H. Schindler, and T. Schmidt, Biophys. J. **73**, 1073 (1997).

20) T. Charitat, E. Bellet-Amalric, G. Fragneto, and F. Graner, Eur. Phys. J. B **8**, 583 (1999).

21) J. Yuan, C. Hao, M. Chen, P. Berini, and S. Zou, (2013).

22) J. T. Marquês, A. S. Viana, and R. F. M. De Almeida, Langmuir **30**, 12627 (2014).

23) F. Okada and K. Morigaki, RSC Adv. **5**, 1507 (2015).

24) J. M. Johnson, T. Ha, S. Chu, and S. G. Boxer, Biophys. J. **83**, 3371 (2002).

25) A. Berquand, P. E. Mazeran, J. Pantigny, V. Proux-Delrouyre, J. M. Laval, and C. Bourdillon, Langmuir **19**, 1700 (2003).

26) R. Tero, M. Takizawa, Y.-J. Li, M. Yamazaki, and T. Urisu, Langmuir **20**, 7526 (2004).

27) P. Lenz, C. M. Ajo-Franklin, and S. G. Boxer, Langmuir **20**, 11092 (2004).

28) R. Tero, N. Misawa, H. Watanabe, S. Yamamura, S. Nambu, Y. Nonogaki, and T. Urisu, E-Journal Surf. Sci. Nanotechnol. **3**, 237 (2005).

29) T. Cha, A. Guo, and X.-Y. Zhu, Biophys. J. **90**, 1270 (2006).

30) T. Isono, H. Tanaka, and T. Ogino, E-Journal Surf. Sci. Nanotechnol. **5**, 99 (2007).

31) C. Kataoka-hamai, H. Inoue, and Y. Miyahara, 9916 (2008).

32) R. Tero, T. Ujihara, and T. Urisu, Langmuir **24**, 11567 (2008).

33) M. P. Krafft and J. G. Riess, Chem. Rev. **109**, 1714 (2009).

34) K. Furukawa, H. Nabika, K. Murakoshi, K. Morigaki, and R. Tero, J. Surf. Sci. Soc. Japan 207 (2009).

35) H. M. Seeger, A. Di Cerbo, A. Alessandrini, and P. Facci, J. Phys. Chem. B **114**, 8926 (2010).

36) Y. Shinozaki, K. Sumitomo, K. Furukawa, H. Miyashita, Y. Tamba, N. Kasai, H. Nakashima, and K. Torimitsu, Appl. Phys. Express **3**, 27002 (2010).

37) R. Tero, G. Sazaki, T. Ujihara, and T. Urisu, Langmuir **27**, 9662 (2011).

38) A. Sumino, T. Dewa, T. Takeuchi, R. Sugiura, N. Sasaki, N. Misawa, R. Tero, T. Urisu, A. T. Gardiner, R. J. Cogdell, H. Hashimoto, and M. Nango, Biomacromolecules **12**, 2850 (2011).

39) S. Ahmed, R. R. Madathingal, S. L. Wunder, Y. Chen, and G. Bothun, Soft Matter **7**, 1936 (2011).

40) X. Zhang and S. Yang, Langmuir 2528 (2011).

41) S. Demarche, K. Sugihara, T. Zambelli, L. Tiefenauer, and J. Vörös, Analyst **136**, 1077 (2011).

42) K. Sugihara, B. Jang, M. Schneider, J. Vörös, and T. Zambelli, Soft Matter **8**, 5525 (2012).

43) Y. Okamoto, K. Tsuzuki, S. Iwasa, R. Ishikawa, A. Sandhu, and R. Tero, J. Phys. Conf. Ser. **352**, 12017 (2012).

44) K. Tsuzuki, Y. Okamoto, S. Iwasa, R. Ishikawa, A. Sandhu, and R. Tero, J. Phys. Conf. Ser. **352**, 12016 (2012).

45) K. Yamazaki, S. Kunii, and T. Ogino, J. Phys. Chem. C **117**, 18913 (2013).

46) T. Isogai, A. Piednoir, E. Akada, Y. Akahoshi, R. Tero, S. Harada, T. Ujihara, and M. Tagawa, J. Cryst. Growth **401**, 494 (2014).

47) A. Sumino, D. Yamamoto, M. Iwamoto, T. Dewa, and S. Oiki, J. Phys. Chem. Lett. **5**, 578 (2014).

48) S. R. Tabaei, J. A. Jackman, B. Liedberg, A. N. Parikh, and N. Cho, J. Am. Chem. Soc. **136**, 16962 (2014).

49) R. Tero, Y. Suda, R. Kato, H. Tanoue, and H. Takikawa, Appl. Phys. Express **7**, 77001 (2014).

50) N. Bag, D. H. X. Yap, and T. Wohland, Biochim. Biophys. Acta - Biomembr. **1838**, 802 (2014).

51) C. Hsieh, S. Spindler, J. Ehrig, and V. Sandoghdar, J. Phys. Chem. B **118**, 1545 (2014).

52) N. Cheng, P. Bao, S. D. Evans, G. J. Leggett, and S. P. Armes, Macromolecules 150416150034001 (2015).

53) Y. Okamoto, T. Motegi, S. Iwasa, A. Sandhu, and R. Tero, Jpn. J. Appl. Phys. **54**, 04DL09 (2015).

54) H. Nabika, A. Sasaki, B. Takimoto, Y. Sawai, S. He, and K. Murakoshi, J. Am. Chem. Soc. **127**, 16786 (2005).

55) K. Suzuki and H. Masuhara, Langmuir **21**, 6487 (2005).

56) H. Nabika, A. Fukasawa, and K. Murakoshi, Langmuir **22**, 10927 (2006).

57) K. Furukawa, K. Sumitomo, H. Nakashima, Y. Kashimura, and K. Torimitsu, Langmuir **23**, 367 (2007).

58) H. Nabika, B. Takimoto, A. Sasaki, A. Fukasawa, and K. Murakoshi, J. Surf. Sci. Soc. Japan **28**, 518 (2007).

59) H. Nabika, B. Takimoto, and K. Murakoshi, Anal. Bioanal. Chem. **391**, 2497 (2008).

60) T. Motegi, H. Nabika, and K. Murakoshi, (2012).

61) K. Furukawa and H. Hibino, Chem. Lett. **41**, 1259 (2012).

62) K. S. Novoselov, A. K. Geim, S. V Morozov, D. Jiang, Y. Zhang, S. V Dubonos, I. V Grigorieva, and A. A. Firsov, Science **306**, 666 (2004).

63) R. R. Nair, P. Blake, A. N. Grigorenko, K. S. Novoselov, T. J. Booth, T. Stauber, N. M. R. Peres, and A. K. Geim, Science **320**, 1308 (2008).

64) L. M. Malard, M. A. Pimenta, G. Dresselhaus, and M. S. Dresselhaus, Phys. Rep. **473**, 51 (2009).

65) T. Tsukamoto and T. Ogino, Appl. Phys. Express **2**, 75502 (2009).

66) Y. Xu, Z. Liu, X. Zhang, Y. Wang, J. Tian, Y. Huang, Y. Ma, X. Zhang, and Y. Chen, Adv. Mater. **21**, 1275 (2009).

67) J. Kim, F. Kim, and J. Huang, Mater. Today **13**, 28 (2010).

68) Y. Zhu, S. Murali, W. Cai, X. Li, J. W. Suk, J. R. Potts, and R. S. Ruoff, Adv. Mater. **22**, 3906 (2010).

69) Y. Iyechika, Sci. Technol. Trends **37**, 76 (2010).

70) H. Zhang, S. Virally, Q. Bao, L. Kian Ping, S. Massar, N. Godbout, and P. Kockaert, Opt. Lett. **37**, 1856 (2012).

71) R. J. Stöhr, R. Kolesov, K. Xia, R. Reuter, J. Meijer, G. Logvenov, and J. Wrachtrup, ACS Nano **6**, 9175 (2012).

72) P. Avouris and C. Dimitrakopoulos, Mater. Today **15**, 86 (2012).

73) J. Rafiee, X. Mi, H. Gullapalli, A. V Thomas, F. Yavari, Y. Shi, P. M. Ajayan, and N. A. Koratkar, Nat. Mater. **11**, 217 (2012).

74) Q. Zheng and J.-K. Kim, *Graphene for Transparent Conductors* (Springer New York, New York, NY, 2015).

75) C. Berger, Z. Song, T. Li, X. Li, A. Y. Ogbazghi, R. Feng, Z. Dai, A. N. Marchenkov, E. H. Conrad, P. N. First, and W. a de Heer, J. Phys. Chem. B **108**, 19912 (2004).

76) T. Ohta, Science **313**, 951 (2006).

77) S. Bae, H. Kim, Y. Lee, X. Xu, J.-S. Park, Y. Zheng, J. Balakrishnan, T. Lei, H. Ri Kim, Y. Il Song, Y.-J. Kim, K. S. Kim, B. Özyilmaz, J.-H. Ahn, B. H. Hong, and S. Iijima, Nat. Nanotechnol. **5**, 574 (2010).

78) K. S. Kim, Y. Zhao, H. Jang, S. Y. Lee, J. M. Kim, K. S. Kim, J.-H. Ahn, P. Kim, J.-Y. Choi, and B. H. Hong, Nature **457**, 706 (2009).

79) L. Gomez De Arco, Y. Zhang, C. W. Schlenker, K. Ryu, M. E. Thompson, and C. Zhou, ACS Nano **4**, 2865 (2010).

80) S. Stankovich, D. A. Dikin, G. H. B. Dommett, K. M. Kohlhaas, E. J. Zimney, E. A. Stach, R. D. Piner, S. T. Nguyen, and R. S. Ruoff, Nature **442**, 282 (2006).

81) V. C. Tung, M. J. Allen, Y. Yang, and R. B. Kaner, Nat. Nanotechnol. **4**, 25 (2009).

82) Y. Gao, X. Chen, H. Xu, Y. Zou, R. Gu, M. Xu, A. K. Y. Jen, and H. Chen, Carbon N. Y. **48**, 4475 (2010).

83) A. Bonanni, A. H. Loo, and M. Pumera, TrAC Trends Anal. Chem. **37**, 12 (2012).

84) V. Georgakilas, J. N. Tiwari, K. C. Kemp, J. A. Perman, A. B. Bourlinos, K. S. Kim, and R. Zboril, Chem. Rev. **116**, 5464 (2016).

85) B. C. Brodie, Philos. Trans. R. Soc. London **149**, 249 (1859).

86) W. S. Hummers and R. E. Offeman, J. Am. Chem. Soc. **80**, 1339 (1958).

87) C.-H. Lu, H.-H. Yang, C.-L. Zhu, X. Chen, and G.-N. Chen, Angew. Chem. Int. Ed. Engl. **48**, 4785 (2009).

88) K. Erickson, R. Erni, Z. Lee, N. Alem, W. Gannett, and A. Zettl, Adv. Mater. **22**, 4467 (2010).

89) E. Morales-Narváez and A. Merkoçi, Adv. Mater. **24**, 3298 (2012).

90) K. P. Loh, Q. Bao, G. Eda, and M. Chhowalla, Nat. Chem. **2**, 1015 (2010).

91) J.-L. Li, H.-C. Bao, X.-L. Hou, L. Sun, X.-G. Wang, and M. Gu, Angew. Chem. Int. Ed. Engl. **51**, 1830 (2012).

92) S. He, B. Song, D. Li, C. Zhu, W. Qi, Y. Wen, L. Wang, S. Song, H. Fang, and C. Fan, Adv. Funct. Mater. **20**, 453 (2010).

93) M. Wu, R. Kempaiah, P.-J. J. Huang, V. Maheshwari, and J. Liu, Langmuir **4**, 2731 (2011).

94) S. Roy, N. Soin, R. Bajpai, D. S. Misra, J. A. McLaughlin, and S. S. Roy, J. Mater. Chem. **21**, 14725 (2011).

95) Y. Wang, Z. Li, D. Hu, C. T. Lin, J. Li, and Y. Lin, J. Am. Chem. Soc. **132**, 9274 (2010).

96) X. Wang, C. Wang, K. Qu, Y. Song, J. Ren, D. Miyoshi, N. Sugimoto, and X. Qu, Adv. Funct. Mater. **20**, 3967 (2010).

97) E. Frotscher, B. Danielczak, C. Vargas, A. Meister, G. Durand, and S. Keller, Angew. Chemie Int. Ed. **54**, 5069 (2015).

98) M. Yoshino, H. Takahashi, T. Takagi, T. Baba, K. Morita, H. Amii, T. Kanamori, and M. Sonoyama, Chem. Lett. **41**, 1495 (2012).

99) H. Takahashi, M. Yoshino, T. Takagi, H. Amii, T. Baba, T. Kanamori, and M. Sonoyama, Chem. Phys. Lett. **559**, 107 (2013).

100) M. Yoshino, T. Kikukawa, H. Takahashi, T. Takagi, Y. Yokoyama, H. Amii, T. Baba, T. Kanamori, and M. Sonoyama, J. Phys. Chem. B **117**, 5422 (2013).

101) C. Zhang, Y. Yuan, S. Zhang, Y. Wang, and Z. Liu, Angew. Chem. Int. Ed. Engl. **50**, 6851 (2011).

102) P.-J. J. Huang and J. Liu, Small **8**, 977 (2012).

103) J. R. Lakowicz, *Principles of Fluorescence Spectroscopy* (Springer US, Boston, MA, 2006).

104) K. Furukawa, H. Nakashima, Y. Kashimura, and K. Torimitsu, Langmuir **24**, 921 (2008).

105) I. L. Medintz and H. Mattoussi, Phys. Chem. Chem. Phys. **11**, 17 (2009).

Chapter 2

Experimental and Theory

Chapter 2. Experimental and Theory

2-1. Preparation of lipid suspension

We prepared the vesicle suspension in the following manner. The chloroform solution of dioleoylphosphatidylcholine (DOPC) was mixed that of other lipids at the required molar ratio into the glass tube. Before using the glass tube was washed with the neutral detergent and was treated with the plasma cleaning to remove the air dust and the carbon residue. The mixed lipid solution was dried with N_2 flow, and overnight evacuation. The vesicle suspension was prepared by suspending the vacuum-dried film of lipid mixture into buffer solution (100 mM KCl, 25 mM HEPES, pH 7.4/NaOH). The obtained multilamellar vesicle suspension was treated with the freezing and thawing by liquid nitrogen and water bath at 45 ˚C, the extrusion using 100 nm polycarbonate filter, and the sonication in water bath to obtain the unilamellar vesicle. We stored the vesicle suspension in a glass vial purged with Ar at 4 ˚C to prevent oxidation of the lipid. Degeneration in membrane morphology or fluidity due to the oxidation of lipid[1,2] was not observed at least during the experimental terms in this study. We used MilliQ water (18.2 MΩ cm at 25 °C) for preparation of all aqueous solutions.

2-2. Formation of supported lipid bilayer

Supported lipid bilayers (SLBs) were prepared by the vesicle fusion method. We incubated a thermally oxidized SiO_2/Si substrate in the unilamellar vesicle suspension under the conditions as follows to prepare SLBs. The SLB was formed by the incubation at 45 ˚C for 60 min. After the incubation, we washed out excess vesicles in a liquid phase by exchanging the suspension

with the buffer solution without vesicles. In the sample for single particle tracking, the substrate was incubated in a cell made of cover glass slips with a spacer of silicone resin. After excess vesicles were removed, the substrate was sealed with the cleaned cover glass.

2-3. Fabrication of graphene oxide

Graphene oxide was prepared following the modified Hummer's method.[3–5] The graphite powder (provided by Ito Kokuen) was stirred at 80 ˚C for 4.5 h in sulfuric acid with potassium persulfate and phosphorus pentoxide, and then was filtrated by the suction filtration using 0.2 μm PTFE filter after cooling to room temperature. After the residue was dried overnight at room temperature, the potassium permanganate was added slowly in the mixture of sulfuric acid with the residue below 10 ˚C. After stirring the mixture at 35 ˚C for 2 h, we added pure water to mixture, and the reaction was quenched by hydrogen peroxide. After precipitating the oxidized graphite overnight, we washed the oxidized graphite with 3% HCl aq. and pure water. The obtained graphite oxide was exfoliated by the centrifugation and the sonication to obtain a single layer GO suspension.

2-4. Apparatus

An epifluorescence microscope (Olympus IX51) was used in bright-field and fluorescence observation. The GO flakes on the SiO_2/Si surface was observed in air. The GO/SiO_2/Si surface after the incubation in vesicle suspension was observed in buffer solution with a 60× water-immersion objective lens. We performed fluorescence recovery after photobleaching (FRAP) by irradiating excitation light 225 times brighter than for observation.

In AFM observation (Agilent PicoScan2500), the GO/SiO_2/Si surface was observed by using a cantilever with spring constant (C) of 28 N/m (SI-DF40, Seiko Instruments Inc.) in acoustic AC mode in the air. The GO/SiO_2/Si surface after the incubation in vesicle suspension was observed by using magnetically coated cantilever (TYPE I MAC Lever, Agilent, C = 0.6 N/m) in magnetic AC mode in the buffer solution.

Single-molecule observation or particle observation for SPT measurement was performed with an inverted fluorescence microscope capable of total-internal reflection illumination (Olympus IX71) equipped with an oil-immersion lens. We adopted a diagonal illumination setup, which enables single molecule imaging on an opaque silicon wafer.[6,7] Samples were illuminated by a 532 nm DPSS laser, and the trajectories of the Rb-DOPE or the Qdot-conjugated lipid were recorded at a time resolution of 30 ms (33 frames per second) or 15.37 ms (67 frames per second) by using an EM-CCD camera (Andor iXon DU-897). The pixel size of the SPT recording was 140.84 nm.

In conventional SPT measurements, fluorescence probes are illuminated by evanescent light resulting from the excitation light introduced from the backside of the substrate at the total internal reflection (TIR) condition (Figure 2-1a). Therefore, substrates are limited to transparent materials such as glass or quartz. In the diagonal illumination setup, the substrate with fluorescence-labeled samples was set upside-down on a cover glass, and illuminated by a light

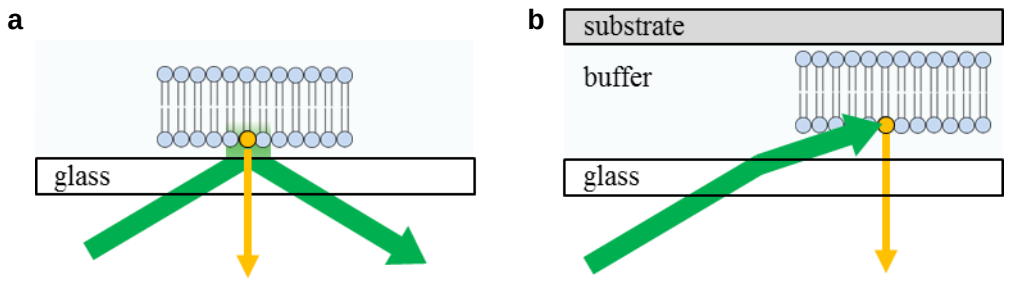

Figure 2-1. Schematic images of (a) the conventional illumination setup with TIR condition and (b) the diagonal illumination setup used in this study.

introduced at the incident angle slightly lower than the TIR condition (Figure 2-1b). This setup enables the SPT measurement of SLB formed on an opaque substrate such as a silicon wafer without limitation on its transparency and refractive index.[1,2)]

2-5. Analysis of molecular diffusion trajectories

The diffusion coefficient (*D*) was obtained by a mean square displacement (MSD) analysis of the diffusion trajectories of dye-labeled lipid (Rb-DOPE) or Qdot-conjugated lipid, which was observed by SPT.[8–11)] We obtained the trajectory coordinates from the movies using ImageJ on the basis of the theory and protocol developed by Sbalzarini and Koumoutsakos.[12)]

The MSD of the trajectories at the time interval of $\tau = n\Delta t$ was calculated by

$$MSD = \langle r(n\Delta t)^2 \rangle = \sum_{i=0}^{N-n-1} \{\vec{r}(i\Delta t + n\Delta t) - \vec{r}(i\Delta t)\}^2 \Big/ \sum_{i=0}^{N-n-1} \quad ,$$

where N is the total number of frames recorded in a movie, Δt is the time resolution of the movie, and $\vec{r}(t)$ is the position vector of the fluorescence probe at time t. MSD was calculated only for the trajectories continuously tracked for longer than 50 frames, because the MSD obtained from a trajectory with larger N has higher statistical reliability. The averaged MSD over many trajectories was the weighted average of the number of frames of each trajectory, obtained by

$$\langle MSD \rangle = \sum_{j=0}^{k-1} \sum_{i=0}^{N_j-n-1} \{\vec{r}(i\Delta t + n\Delta t) - \vec{r}(i\Delta t)\}^2 \Big/ \sum_{j=0}^{k-1} \sum_{i=0}^{N_j-n-1} \quad ,$$

where k is the number of trajectories over which the average is calculated (trajectory 0, trajectory 1, ..., trajectory k-1), and N_j is the total number of frames of the trajectory j.[13)] We plotted MSD or $\langle$MSD$\rangle$ against τ to obtain D, because MSD is expressed as a linear function

following

$$\mathrm{MSD} = 4D\tau \qquad (1)$$

for random diffusion.

2-6. Evaluation of molecular interaction based on Arrhenius plot

Prior studies showed that the temperature dependence of D of a lipid molecule in a homogeneous lipid bilayer membrane is expressed on the basis of the free-volume theory.[14–16] According to the theory derived by Schram and Hall,[17] the temperature dependence of D is expressed as

$$D = A_0 \exp\left(-\frac{E'_a}{RT}\right), \qquad (2)$$

where E'_a is the apparent activation energy in the unit of J/mol, R is the molar gas constant, T is temperature. The preexponential factor A_0 is a constant determined by the cross section area and molecular weight of the lipid. E'_a depends only on the activation energy E_a and the area thermal expansion coefficient α as follows:

$$E'_a = E_a + (R/\alpha) - c \qquad (3)$$

where c is a temperature-independent constant. E'_a is obtained from the conventional Arrhenius plot of D,

$$\ln D = -E'_a/RT + \ln A_0. \qquad (4)$$

Reference

1) A. G. Ayuyan and F. S. Cohen, Biophys. J. **91**, 2172 (2006).

2) Y. Suda, R. Tero, R. Yamashita, K. Yusa, and H. Takikawa, Jpn. J. Appl. Phys. **55**, 03DF05 (2016).

3) W. S. Hummers and R. E. Offeman, J. Am. Chem. Soc. **80**, 1339 (1958).

4) R. Ishikawa, M. Bando, Y. Morimoto, S. Y. Park, and A. Sandhu, Jpn. J. Appl. Phys. **49**, 12 (2010).

5) Y. Okamoto, K. Tsuzuki, S. Iwasa, R. Ishikawa, A. Sandhu, and R. Tero, J. Phys. Conf. Ser. **352**, 12017 (2012).

6) R. Tero, G. Sazaki, T. Ujihara, and T. Urisu, Langmuir **27**, 9662 (2011).

7) Y. Okamoto, T. Motegi, S. Iwasa, A. Sandhu, and R. Tero, Jpn. J. Appl. Phys. **54**, 04DL09 (2015).

8) D. D. Gross and W. W. Webb, in *Spectrosc. Membr. Probes Vol. II*, edited by L. M. Loew (CRC Press, Boca Raton, FL, 1988), pp. 19–45.

9) G. J. Schütz, H. Schindler, and T. Schmidt, Biophys. J. **73**, 1073 (1997).

10) A. Sergé, N. Bertaux, H. Rigneault, and D. Marguet, Nat. Methods **5**, 687 (2008).

11) R. Metzler, J.-H. Jeon, A. G. Cherstvy, and E. Barkai, Phys. Chem. Chem. Phys. **16**, 24128 (2014).

12) I. F. Sbalzarini and P. Koumoutsakos, J. Struct. Biol. **151**, 182 (2005).

13) R. Tero, G. Sazaki, T. Ujihara, and T. Urisu, Langmuir **27**, 9662 (2011).

14) P. F. F. Almeida and W. L. C. Vaz, in *Handb. Biol. Phys.*, edited by R. Lipowsky and E. Sackmann (Elsevier, 1995), pp. 305–357.

15) V. Schram and S. B. Hall, Biophys. J. **86**, 3734 (2004).

16) M. D. King and D. Marsh, Biochim. Biophys. Acta - Biomembr. **862**, 231 (1986).

17) V. Schram and S. B. Hall, Biophys. J. **86**, 3734 (2004).

Chapter 3

Fabrication of artificial lipid bilayer membrane on graphene oxide

Chapter 3. Fabrication of artificial lipid bilayer membrane on graphene oxide

3-1. Introduction

A lipid bilayer is the fundamental structure of plasma membranes. The lipid bilayer is not only a static wall between the inside and outside of cell, but also has important functions, such as the transportation of small molecules, ions, and signals into and out of cells through specific channels and endo- and exocytosis, through the two-dimensional organization and molecular diffusion.[1,2] The behavior of lipids and proteins in plasma membranes and their relation with the functions during reactions have been studied extensively.[2–4] Supported lipid bilayers (SLBs), which are artificial bilayer membrane at solid-liquid interfaces, have been investigated as cell membrane models to study the physicochemical properties of lipid bilayers, and as the platform for membrane proteins.[5,6] Recently, some new methods were reported to obtain detailed information of biochemical molecules using graphene and graphene oxide (GO).[7–11] Our purpose is the development of a new method to obtain detailed information of biomolecules on and in plasma membranes, using graphene-supported lipid bilayers (G-SLBs). We prepared the SLB of phosphatidylcholine on GO by the vesicle fusion method.[12–16]

At the formation of SLB by the vesicle fusion method, the efficiency of the formation of planar membranes depends on the material, shape and chemical states of substrate surfaces.[15–17] It is necessary to establish a reproducible condition for the formation of SLB on GO. GO has amphiphilicity, because GO consists of the hydrophilic sp^3-carbon regions including –OH, –O–, and –COOH groups, and of the hydrophobic sp^2-carbon regions, which are close to perfect graphene.[18–20] A lipid bilayer is a self-assembled structure of amphiphilic lipid molecules.

Therefore, the behavior of lipid bilayers on the amphiphilic GO surface is an interesting subject from the view point of interfacial chemistry. In this manuscript, we describe the formation of SLB by vesicle fusion method, and the effect of vesicle size and Ca^{2+} ion.

3-2. Specific experimental condition

GO suspension was prepared from graphite powder (Z+80, Ito Kokuen Co., Ltd., Japan) by chemical exfoliation according to the modified Hummer's method as mentioned in Section 3, Chapter 2.[21–23] The width of the GO flakes before sonication was 213 μm at maximum (Figure 3-1a). The size of the GO flakes became 1-10 μm after the sonication. The height of the GO flakes on the SiO_2/Si surface obtained from AFM topography was 1.74 ± 0.20 nm (n=40) (Figure 3-1b, and 3-1c).

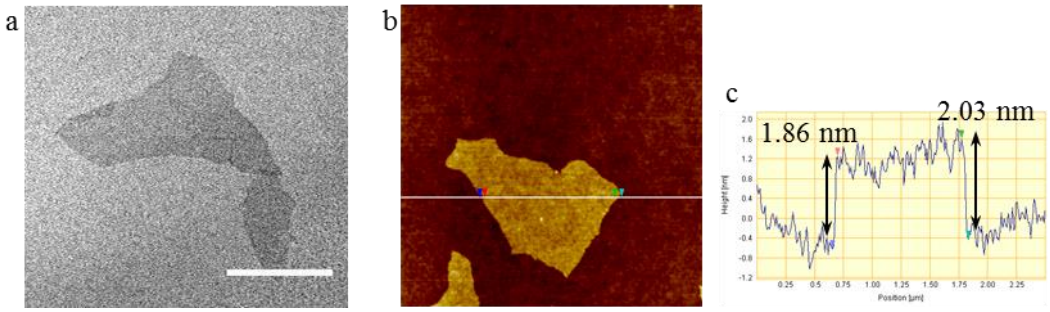

Figure 3-1. (a) Bright field image of GO on SiO_2/Si. Scale bar correspond to 100 μm. (b) AFM topography of GO after sonication dropcast on SiO_2/Si. Image size is 2.5×2.5 μm^2. (c) Cross section profile at the white line in (b).

The vesicle suspension was prepared as mentioned in Section 1, Chapter 2. The chloroform solution of dioleoylphosphatidylcholine (DOPC) (Avanti Pola Lipid) and the ethanol solution of fluorescence-labeled lipid (BOPIPY-H-PC: Ex/Em = 534/552 nm) (Invitrogen) were mixed at 100:1 molar ratios in a glass vial. SLB was formed on the GO/SiO_2/Si substrate by vesicle fusion method as mentioned in Section 2, Chapter 2.

3-3. Results and discussion

Figure 3-2a shows the AFM topography of the GO/SiO_2 surface after the incubation in the 100 nm-extruded vesicle suspensions. Generally, a full-coverage SLB can be obtained on SiO_2 using 100 nm-extruded vesicle suspensions.[12,13] The GO regions in Figure 3-2a, however, were covered with 13 nm-high protrusions, which were assigned to unruptured vesicles.[14] The transformation from vesicles to SLB did not proceed on GO. From the previous results, it is known that the formation of SLB are assisted if vesicle sizes were decreased by sonication, and/or Ca^{2+} ion was added into buffer solutions.[12,13] Therefore, we studied the effect of the pre-sonication of the vesicle suspension and of the addition of Ca^{2+} ion in the buffer solution on the formation of the DOPC-SLB on the GO/SiO_2 surface (Figure 3-2).

Figure 3-2b shows the AFM topography of the GO/SiO_2/Si surface after the incubation in sonicated vesicle suspension. Although a few flat regions were observed on GO, the majority of the GO surface was covered with 16 nm-high protrusion, which were also assigned to the unruptured vesicles. Figure 3-2c and 3-2d show the AFM topographies of the GO/SiO_2/Si surface after the incubation in vesicle suspension containing 5 mM of $CaCl_2$. We observed flat morphology on both GO and SiO_2 regions with both the 100 nm-extruded vesicle suspension (Figure 3-2c) and the sonicated vesicle suspension (Figure 3-2d). We found few large protrusions observed in Figure 3-2a and 3-2b. The surface of each GO flake was flat, the height within each GO flake was constant, and the GO regions were always higher than the SiO_2 regions. These results suggest that SLB was formed on GO. In Figure 3-2c, the height of the GO regions from the SiO_2 regions was 6.86 ± 0.73 nm (n = 40). In Figure 3-2d, the height of the GO regions from the SiO_2 regions were 1.55 ± 0.28 nm (n = 60), or 5.61 ± 0.58 (n = 60).

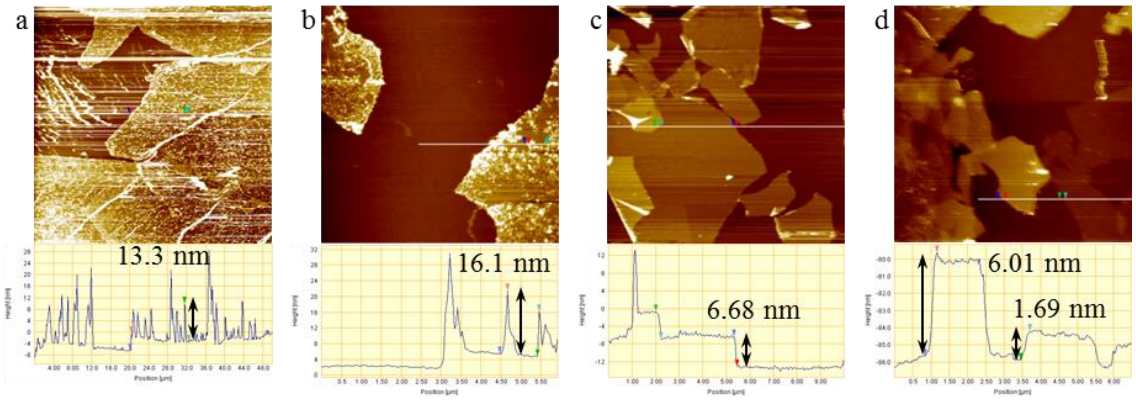

Figure 3-2. AFM topographies of the GO/SiO_2 surfaces after incubated at typical condition, and the cross section profiles at the white line in each AFM topography. (a) Vesicle suspension without sonication in the absence of $CaCl_2$. (b) Sonicated vesicle suspension in the absence of $CaCl_2$. (c) Vesicle suspension without sonication in the presence of 5 mM $CaCl_2$. (d) Sonicated vesicle suspension in the presence of 5 mM $CaCl_2$. Image sizes are (a) 50×50 μm^2, and (b-d) 10×10 μm^2.

Figure 3-3 shows the fluorescence images of the SLB/GO/SiO_2 surface incubated under the same condition as Figure 3-2d. The SLB formed on GO was remarkably darker than that on SiO_2. This result confirmed that the fluorescence from the BODIPY-H-PC in the DOPC-SLBs was quenched by GO.[24–26] We performed FRAP to study the fluidity of the SLB on GO. After the SiO_2 regions surrounding by GO (Figure 3-3a, dotted circle) was photobleached, the fluorescence at the SiO_2 regions recovered with time (Figure 3-3b, 3-3c, and 3-3d). This result indicates that lipid molecules diffused freely between the SiO_2 regions and the surrounding GO regions, therefore that fluid and continuous SLB were formed on GO, as well as on SiO_2.

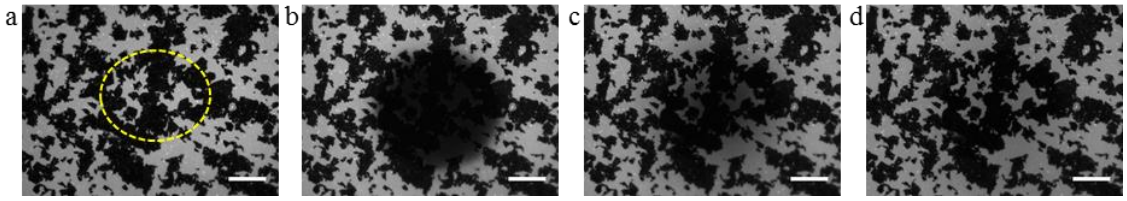

Figure 3-3. Fluorescence images of the GO-supported lipid bilayers and FRAP process. (a) Before fluorescence bleaching. (b) 0 s, (c) 180 s, and (d) 600 s after photobleaching. Scale bars correspond to 20 μm.

Figure 3-4 shows the structural model of SLB/GO system, which we propose based on the height, observed in the AFM topography (Figure 3-2d) and the result of FRAP (Figure 3-3). The SLB on the SiO_2 regions had fluorescence, and FRAP proceeded. This result indicates that single lipid bilayer was formed on SiO_2 similarly to previous studies.[13,15)] Single lipid bilayer was also formed on GO, because the height of the GO regions, which was 1.6 nm from SLB/SiO_2, was close to the height of GO in Figure 3-1. On the other hand, the GO regions 5.6 nm higher than the SLB/SiO_2 was 4.0 nm higher than the single SLB/GO regions. This value corresponded to the thickness of single lipid bilayer observed by AFM. Previous AFM studies show that the thickness of DOPC-SLB observed with tapping mode is 4-5 nm.[27–30)] Hence we conclude that two layers of lipid bilayer were formed on GO. Furthermore, the results of FRAP measurement (Figure 3-3) suggests that the lipid bilayers on GO and SiO_2 had fluidity and continuity.

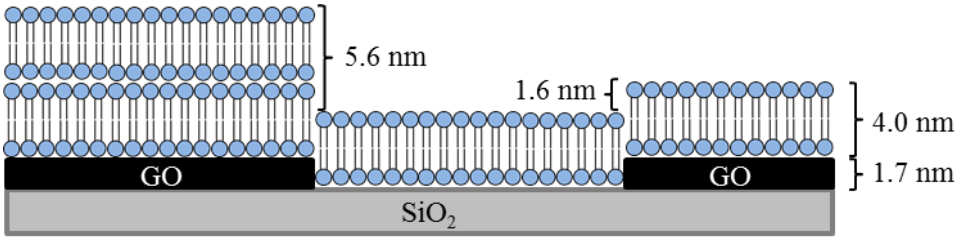

Figure 3-4. Structural model of the SLB/GO/SiO_2 system.

The spontaneous formation of double SLBs on GO by vesicle fusion is a unique phenomenon to GO. Generally, only single SLB is formed on homogeneously hydrophilic oxide surfaces (e.g. SiO_2, mica, TiO_2, etc.) by vesicle fusion method. The reason why only single SLB is formed on the oxide surfaces is not clear, even though multilamellar lipid bilayers are thermally stable.[30)] The process of the transformation from adsorbed vesicle to planar membrane at the vesicle fusion method has highly kinetic aspects.[12,13)] The layer number of the formed SLB may be related to the membrane formation mechanism of the vesicle fusion method. The GO surface is

heterogeneous, because it consists of the hydrophilic regions including hydroxyl, epoxy and carboxyl groups, and of the hydrophobic regions close to perfect graphene.[20] The transformation from vesicles to SLB may proceed through a different mechanism from the homogeneously hydrophilic oxide surfaces. If we consider the application of SLBs as a platform for membrane protein research, direct interaction between the solid surface and the proteins incorporated in the SLB, especially their extramembrane regions should be avoided. One of strategies for this problem is "tethered lipid bilayer", lipid bilayers linked with the substrate surface to make a space between the lipid bilayer and substrate.[31–34] The double SLB system on GO may provide another methodology: the first SLB on GO may work as a buffer between the substrate and the extramembrane region of the proteins incorporated in the second lipid membrane, because PC-SLB prevents non-specific adsorption of proteins.

3-4. Summary

We prepared DOPC-SLB on the GO/SiO_2/Si surface by the vesicle fusion method. Fluid and planar lipid bilayers were formed on GO after the incubation of GO on the thermally oxidized SiO_2/Si substrate in $CaCl_2$-containing DOPC vesicle suspension. From the AFM observation, we found that not only single lipid bilayer, similar to inorganic substrates, but also double lipid bilayers were formed on GO. We proposed a structural model of the GO-SLB system. This GO-SLB system is the fundamental platform for the measurement of biomolecules in the plasma membrane model using graphene.

Reference

1) H. Hirayama, J. Memb. Sci. **139**, 109 (1998).

2) R. G. W. Anderson and K. Jacobson, Science **296**, 1821 (2002).

3) K. Jacobson, O. G. Mouritsen, and R. G. W. Anderson, Nat. Cell Biol. **9**, 7 (2007).

4) D. Lingwood and K. Simons, Science **327**, 46 (2010).

5) A. Hirano-Iwata, M. Niwano, and M. Sugawara, TrAC Trends Anal. Chem. **27**, 512 (2008).

6) T. Cha, A. Guo, and X.-Y. Zhu, Biophys. J. **90**, 1270 (2006).

7) C.-H. Lu, H.-H. Yang, C.-L. Zhu, X. Chen, and G.-N. Chen, Angew. Chem. Int. Ed. Engl. **48**, 4785 (2009).

8) S. He, B. Song, D. Li, C. Zhu, W. Qi, Y. Wen, L. Wang, S. Song, H. Fang, and C. Fan, Adv. Funct. Mater. **20**, 453 (2010).

9) P. K. Ang, M. Jaiswal, C. H. Y. X. Lim, Y. Wang, J. Sankaran, A. Li, C. T. Lim, T. Wohland, O. Barbaros, and K. P. Loh, ACS Nano **4**, 7387 (2010).

10) M. Wu, R. Kempaiah, P.-J. J. Huang, V. Maheshwari, and J. Liu, Langmuir **4**, 2731 (2011).

11) X. Wang, C. Wang, K. Qu, Y. Song, J. Ren, D. Miyoshi, N. Sugimoto, and X. Qu, Adv. Funct. Mater. **20**, 3967 (2010).

12) I. Reviakine and A. Brisson, Langmuir **16**, 1806 (2000).

13) R. Tero, T. Ujihara, and T. Urisu, Langmuir **24**, 11567 (2008).

14) R. Tero, H. Watanabe, and T. Urisu, Phys. Chem. Chem. Phys. **8**, 3885 (2006).

15) T. Isono, H. Tanaka, and T. Ogino, E-Journal Surf. Sci. Nanotechnol. **5**, 99 (2007).

16) R. Tero, M. Takizawa, Y.-J. Li, M. Yamazaki, and T. Urisu, Langmuir **20**, 7526 (2004).

17) R. P. Richter, R. Bérat, and A. R. Brisson, Langmuir **22**, 3497 (2006).

18) C. Gómez-Navarro, J. C. Meyer, R. S. Sundaram, A. Chuvilin, S. Kurasch, M. Burghard, K. Kern, and U. Kaiser, Nano Lett. **10**, 1144 (2010).

19) K. Erickson, R. Erni, Z. Lee, N. Alem, W. Gannett, and A. Zettl, Adv. Mater. **22**, 4467 (2010).

20) K. P. Loh, Q. Bao, G. Eda, and M. Chhowalla, Nat. Chem. **2**, 1015 (2010).

21) R. Ishikawa, M. Bando, Y. Morimoto, S. Y. Park, and A. Sandhu, Jpn. J. Appl. Phys. **49**, 12 (2010).

22) Y. Gao, X. Chen, H. Xu, Y. Zou, R. Gu, M. Xu, A. K. Y. Jen, and H. Chen, Carbon N. Y. **48**, 4475 (2010).

23) V. C. Tung, M. J. Allen, Y. Yang, and R. B. Kaner, Nat. Nanotechnol. **4**, 25 (2009).

24) J. Kim, F. Kim, and J. Huang, Mater. Today **13**, 28 (2010).

25) R. S. Swathi and K. L. Sebastian, J. Chem. Phys. **130**, 86101 (2009).

26) R. S. Swathi and K. L. Sebastian, J. Chem. Phys. **129**, 54703 (2008).

27) E. I. Goksu, J. M. Vanegas, C. D. Blanchette, W.-C. Lin, and M. L. Longo, Biochim. Biophys. Acta **1788**, 254 (2009).

28) J. T. Marquês, A. S. Viana, and R. F. M. De Almeida, Biochim. Biophys. Acta **1808**, 405 (2011).

29) P.-E. Milhiet, F. Gubellini, A. Berquand, P. Dosset, J.-L. Rigaud, C. Le

Grimellec, and D. Lévy, Biophys. J. **91**, 3268 (2006).

30) F. Domenici, D. Panichelli, and A. C. Castellano, Colloids Surf. B. Biointerfaces **69**, 216 (2009).

31) R. Tero, N. Misawa, H. Watanabe, S. Yamamura, S. Nambu, Y. Nonogaki, and T. Urisu, E-Journal Surf. Sci. Nanotechnol. **3**, 237 (2005).

32) S. Lei, R. Tero, N. Misawa, S. Yamamura, L. Wan, and T. Urisu, Chem. Phys. Lett. **429**, 244 (2006).

33) W. Knoll, H. Park, E. Sinner, D. Yao, and F. Yu, Surf. Sci. **570**, 30 (2004).

34) S. Terrettaz, M. Mayer, and H. Vogel, Langmuir **19**, 5567 (2003).

Chapter 4

Modification of lipid bilayers with quantum dots for single particle tracking

Chapter 4. Modification of lipid bilayers with quantum dots for single particle tracking

4-1. Introduction

The lipid bilayer is a fundamental structure of plasma membranes and plays important roles in membrane reactions such as the transport of material, information, and energy into and out of cells.[1–3] Supported lipid bilayers (SLBs) are one of the artificial lipid membrane systems formed at solid-liquid interfaces.[4–6] The artificial lipid membranes have been investigated as cell membrane models to study the structure and physicochemical properties of lipid bilayers and the effects of chemical and/or artificial materials on them.[7–13] The SLBs are also valuable as a platform for investigating the function of membrane proteins,[14–17] because the two dimensional assembly and physical properties of lipids around the membrane proteins significantly affect the activity of the proteins.[1] The membrane proteins are also important targets in the medical field, thus a new approach to measure the molecular dynamics in the lipid bilayer are demanded.

Recently, various biological applications making use of the unique physical and electronic properties of graphene and graphene oxide(GO) were reported.[18–24] Graphene is a single atomic sheet of aromatic carbons, and GO is the derivative of graphene with oxygen functional groups such as hydroxyl, epoxy, and carboxyl groups on its surface.[25–29] Graphene and GO have a unique fluorescence quenching ability. The quenching by graphene and GO is independent of the wavelength of donor fluorescence probe, and the effective range which is expressed as the Förster radius, is longer than those of general quencher molecules.[30] In particular, GO is hydrophilic because of the epoxy, hydroxyl, and carboxyl groups on its surface, and is therefore

applied to the sensing of biological binding reactions such as DNA hybridization, antigen-antibody reaction, and aptamer binding.[21,22,31)]

Lipid bilayers are also targets for the sensing technique using graphene and GO, and there are reports on the interaction of the lipid bilayer formed on graphene and GO.[32–36)] Frost et al. reported the assembly of a multilayered structure of positively charged lipid membranes and GO consisting of alternating GO sheets and the lipid membranes because of electrostatic interaction.[32)] Previously we investigated the formation of the planar lipid membranes of a neutral phospholipid on GO and chemically reduced GO, and established a fabrication protocol of SLBs on GO by the vesicle fusion method.[34,35)] We found that multilayered SLBs were formed on GO as well as single SLB layers by atomic force microscope (AFM) observation,[35)] while generally only single SLB was formed on solid supports by the vesicle fusion method.[6)] We showed that the SLBs formed on GO has fluidity, referring to the result of fluorescence recovery after photobleaching (FRAP) measurement. However, we could not evaluated this fluidity quantitatively because of the strong fluorescence quenching of GO. In this study, we conjugated quantum dots (Qdots) as they are a brighter probe than dye molecules to the surface of SLBs, in order to evaluate the fluidity of the SLB on GO quantitatively. We could detect the fluorescence signal from Qdot-conjugated lipids even on the SLB on GO by single-particle tracking (SPT). The addition of a lipid modified with polyethylene glycol effectively prevented unspecific adsorption of the Qdot onto the SLB surface. We evaluated the diffusion coefficient of the Qdot-conjugated lipids from their diffusion trajectories obtained by SPT, by the mean-square displacement (MSD) analysis. We presented the difference in the lipid diffusion behavior between the SLB formed on GO and that on SiO_2/Si as the diffusion coefficient of single Qdot-conjugated lipid diffusing between the GO region and the SiO_2 region.

4-2. Specific experimental condition

The vesicle suspension was prepared according the previous mentioned method in Section 1, Chapter 2. The chloroform solution of dioleoylphosphatidylcholine (DOPC) mixed with that of dioleoylphosphatidylethanolamine-N-(lissamine rhodamine B sulfonyl) (Rb-DOPE, E_x/E_m = 557/571 nm) as the fluorescence probe, dipalmitoylphosphatidylthioethanol (DPPTE), and 1,2-distearoyl-sn-glycero-3-phosphoethanol-amin-N-[amino(polyethylene glycol)-2000] (PEG-DSPE) at the required molar ratio. DOPC-SLB without pegylated lipid was contained 1×10^{-6}% DPPTE for Q-dot conjugation, or 1×10^{-6}% Rb-DOPE. The DOPC-SLB with pegylated lipid contained 5% PEG-DSPE, and 5×10^{-7}% DPPTE for SPT, and additionally 0.2% Rb-DOPE for FRAP measurement.

Graphene oxide was prepared following the modified Hummer's method[35,37,38] mentioned in Section 3, Chapter 2.

We prepared the SLB on the SiO_2/Si substrates with or without GO deposition by the vesicle fusion method[35,39,40] mentioned in Section 2, Chapter 2.

A carboxyl-coated Qdot (Lifetechnologies) was modified with a maleimide-hydrazide hetero-cross-linker (Quanta BioDesign) and 2-(2-aminoethoxy) ethanol (AEE) using 1-ethyl-3-(3-dimethylaminopropyl) carbodiimide (EDC), and then added to a SLB containing thiol-terminated lipid (DPPTE).[41] AEE was coadsorbed with the cross-linker to control the number of efficient maleimide groups on the Qdot surface for the covalent formation with DPPTE in the SLB, and to suppress the multivalent and/or nonspecific adsorption of the Qdot.

The diffusion coefficient (*D*) was obtained based on the MSD analysis of the trajectories of dye-labeled lipid (Rb-DOPE) or Qdot-labeled lipid observed by SPT mentioned in Section 5, Chapter 2.

4-3. Results and discussion

Figures 4-1a and 4-1b show the result of the SPT measurement of the DOPC-SLB on GO/SiO_2/Si using a fluorescence-labeled lipid (Rb-DOPE) as a probe. We observed bright spots corresponding to fluorescence signals from each Rb-DOPE molecule in the SiO_2 region, but not in the GO region (Figure 4-1a). We observed the molecular diffusion of Rb-DOPE between the GO region and SiO_2 region (Figure 4-1b). The fluorescence signal of the Rb-DOPE molecule suddenly appeared in a SiO_2 region at the border on GO (Figure 4-1b, 0.09 s), diffused around in the SiO_2 region for a short time, and disappeared at the border on GO (Figure 4-1b, 0.55s). This result indicates that quenched Rb-DOPE in the SLB on GO diffused from the GO region to the SiO_2 region. It suggests that the SLB formed on GO has fluidity, and continues to that on SiO_2. The result is consistent with our previous work, in which we found that in the DOPC-SLB/GO/SiO_2 system, the SLBs formed on the GO and SiO_2 regions are continuous and lipid molecules freely diffuse into and out of two regions, thorough macroscopic fluidity measurement by the FRAP method. However, we could not detect the fluorescence signal from the Rb-DOPE in the SLB on GO because of the high efficiency of quenching by GO (Figure 4-1c).

To evaluate the fluidity of the SLB on GO quantitatively, a fluorescence probe bright enough to observe the fluorescence signal even under the effect of fluorescence quenching of GO is necessary. Note that in the SPT experiment the long accumulation time does not improve the signal intensity, because the lipids do not stay at the same position in the SLB. Therefore, we used a Qdot as such a brighter fluorescence probe. We covalently conjugated a carboxyl-terminated Qdot to the SLB containing DPPTE via a hetero-cross-linker with amino and maleimide groups. Figure 4-1d is the fluorescence image of DOPC-SLB containing DPPTE

after the modification with Qdot. It shows that the Qdot is bright enough for SPT measurement even under the effect of fluorescence quenching by GO. In this image, however, many immobile Qdots also exist. We observed several diffusing Qdots in both SiO_2 and GO regions, but the majority of the Qdots were immobile probably because of the nonspecific adsorption of Qdots on the surface of the SLB, and/or because of multivalent bonding between a Qdot and several DPPTE molecules in the SLB.

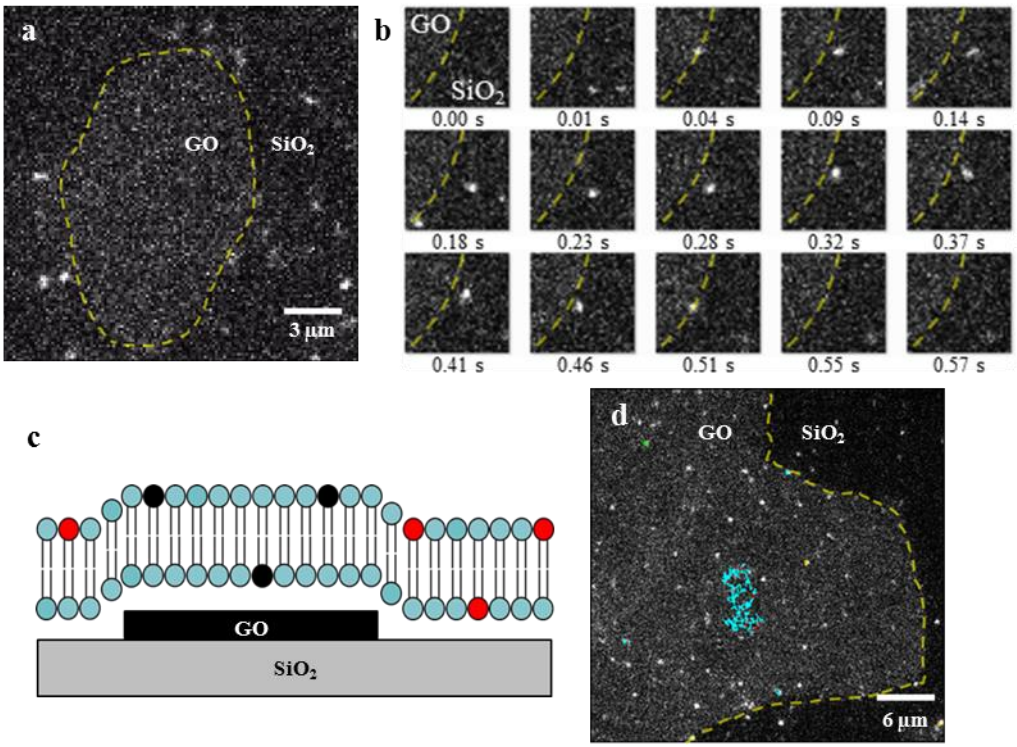

Figure 4-1. (a) Fluorescence single-molecule image of SLB containing Rb-DOPE on $GO/SiO_2/Si$, and (b) captured images of Rb-DOPE diffusing between the GO region and SiO_2 region. (c) Schematic illustration of SLB/GO system. (d) Fluorescence single-molecule image of Qdot conjugated with SLB on GO, and its trajectory (blue trace).

Figure 4-2a shows the trajectory of a Qdot conjugated to the DOPC-SLB containing DPPTE on a SiO_2/Si substrate without GO. We evaluated the diffusion behavior of the Qdot-conjugated lipids by the MSD analysis of 90 trajectories (Figure 4-2b). The value of *D* was obtained for each trajectory by the linear fitting with Eq. (1). The histogram of *D* shows a wide distribution

(Figure 4-2c), and the average of D is 0.44 μm^2/s. This value of D is significantly smaller than that of single-dye-labeled lipid in SLB, for example, 2.53 μm^2/s is reported under similar experimental conditions to those in the current study.[42] The larger size of the Qdot, which exists in an aqueous solution above SLB, than a fluorescence dye molecule rarely affects D, because the membrane fluidity is mainly dominated by the hydrophobic part, which has higher viscosity than those of water by a factor of = 100.[43] Therefore, the result suggests that multivalent bonds were formed between the Qdots and the DPPTE molecules in the SLB. Thus, it is difficult to compare D between the SiO_2 and GO regions determined using different Qdot-conjugated

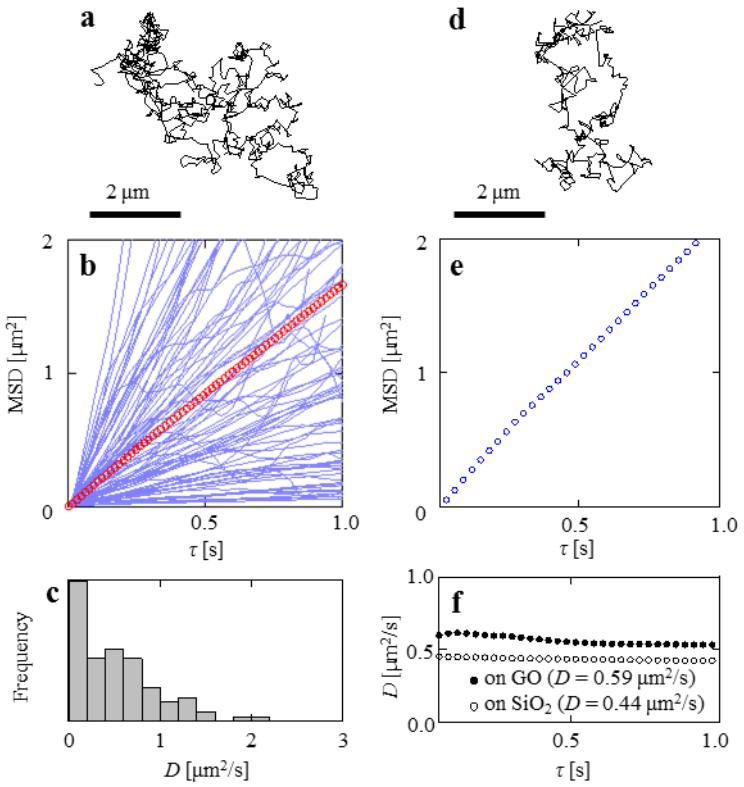

Figure 4-2. (a) Trajectory of Qdot-conjugated lipids in the DOPC-SLB on the SiO_2/Si substrate. (b) MSD-τ plot of all trajectories obtained in the sample of (a). Blue lines are MSD of each trajectory, and red circle is the average MSD obtained from all trajectories. (c) D-histogram calculated from all trajectories in (a). (d) Trajectory of single Qdot-conjugated lipid in the SLB on GO. (e) MSD-τ plot of the trajectory in (d). (f) D-τ plots obtained from the average MSD in (b) (white circle) and from the MSD of single Qdot-conjugated lipid in (e) (black circle).

lipids.

Figure 4-2d shows a trajectory of a Qdot conjugated to the DOPC-SLB containing DPPTE on the GO-deposited SiO_2/Si substrate. We observed a few diffusing Qdots on the SLB on GO. We obtained a trajectory long enough to reliably evaluate *D* by the MSD analysis of a single trajectory of one Qdot because of the long lifetime before photobleaching of Qdots (for example, 498 frames for the movie in Figure 4-2d). The value of *D* obtained from the single Qdot-conjugated lipid on the GO region was 0.59 $\mu m^2/s$ (Figure 4-2e). Figure 4-2f shows D-τ plots of the trajectories of Qdots on the SiO_2 region and the GO region. From the D-τ plot, we can obtain the information about the spatiotemporal diffusion behavior, such as a normal diffusion and anomalous diffusion. In the case of anomalous diffusion, *D* changes with τ in the heterogeneous environments such as those with corrals or obstacles.[42,44,45] Figure 4-2f shows that *D* is independent of τ in the SLBs on both SiO_2 and GO regions. This result indicates that the Qdot-conjugated lipids diffused by normal diffusion (Brownian motion) in the SLB formed on both SiO_2 and GO. Therefore, we infer that the SLB on GO was homogeneous without the inner lipid structure, at least in this spatiotemporal range.

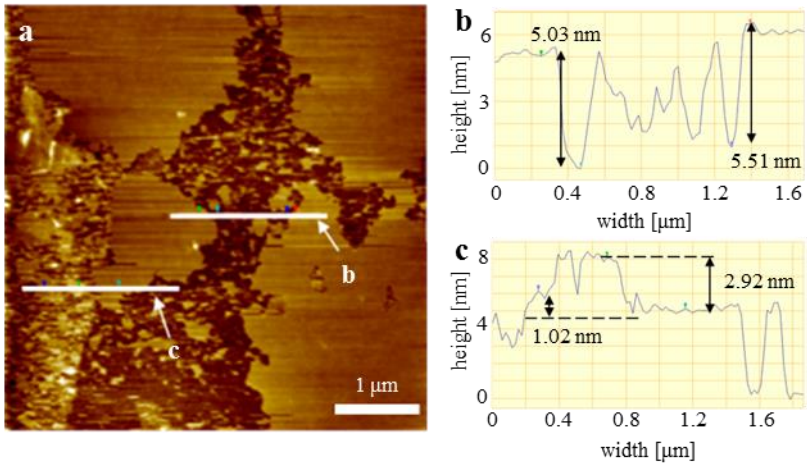

Figure 4-3. (a) AFM topography image (4.0×4.0 μm^2) of the DOPC-SLB containing 5% PEG-DSPE formed on GO/SiO_2. (b), (c) Cross-sectional profiles along the white lines in (a).

To suppress the nonspecific adsorption of Qdot to the SLB surface, we prepared the SLB containing 5 mol% PEG-DSPE, as well as DPPTE. Figure 4-3a shows the AFM topography image of the surface of the pegylated SLB formed on the GO-deposited SiO_2 under the condition of submonolayer SLB formation. We observed flat morphology on the SLB on the bare SiO_2 region, and the height from the SiO_2 surface to the SLB surface was 5.1 ± 0.99 nm (n = 7) (Figure 4-3b). In the GO region, a part of the GO surface was still exposed because the formation of the SLB was not complete. Two regions with different heights existed in the SLB on GO, and they were higher than the SLB on the SiO_2 region by ~3 and ~1 nm (Figure 4-3c). This result suggests that two kinds of domains existed after the SLB formation process.

To check the fluidity of pegylated SLB formed on GO, we performed the FRAP measurement using an epi-fluorescence microscope. Figure 4-4 shows the fluorescence images of the pegylated SLB containing 0.2 mol% dye-labeled lipid formed on the GO-deposited SiO_2/Si surface. Because the fluorescence signal from dye-labeled lipid in the SLB on GO was not detected owing to fluorescence quenching of GO, the FRAP measurement was performed for the SLB on a bare SiO_2 region surrounded by GO regions. The fluorescence intensity in the SiO_2 region recovered with time. This indicates that bright dye-labeled lipids were supplied from the surrounding GO region to the bleached SiO_2 region by lateral molecular diffusion. Therefore, this result suggests that the pegylated SLB on GO retained fluidity, and was continuous with the SLB on the SiO_2 region, as similar to DOPC-SLB.[35)]

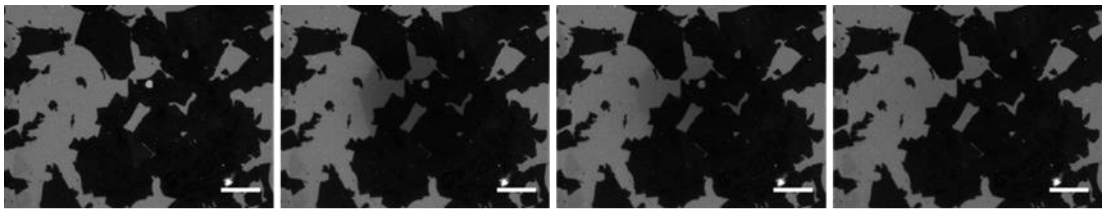

Figure 4-4. Fluorescence images of the DOPC-SLB containing 5% PEG-DSPE subjected to FRAP process. Scale bar is 20 μm.

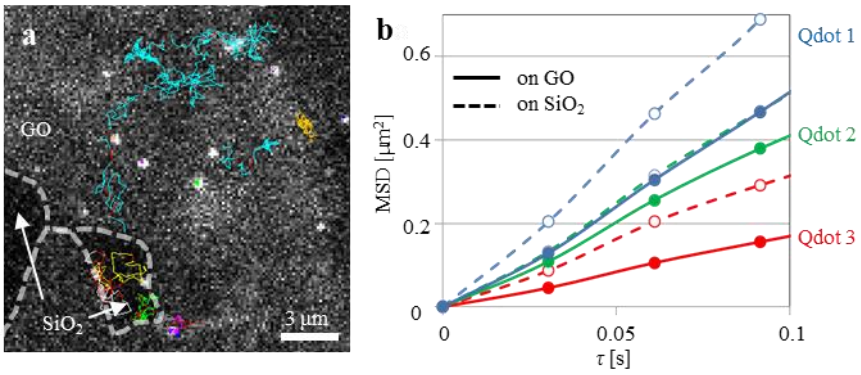

Figure 4-5. (a) Fluorescence single-particle tracking of Qdot-conjugated lipid in the DPPTE-containing DOPC-SLB with 5% PEG-DSPE. (b)MSD-τ plot of single Qdot-conjugated lipid diffusing on GO (filled circle) and on SiO_2 (blank circle).

We indirectly confirmed the fluidity of the pegylated SLB on GO in the FRAP measurement in Figure 4-4. Then we performed the SPT measurement after the conjugation of the Qdot to the pegylated SLB containing 5×10^{-7}% DPPTE on the GO/SiO_2/Si substrate to evaluate the fluidity quantitatively. The diffusion of Qdot-conjugated lipids was observed in both the GO region and the SiO_2 region (Figure 4-5a). The number of immobile Qdots was significantly suppressed in comparison with that in the SLB without PEG-DSPE shown in Figure 4-1d. More importantly, we observed the diffusion of Qdot-conjugated lipids between the GO region and the SiO_2 region. We are able to evaluate the difference in fluidity between the SLBs on GO and on SiO_2, by comparing *D* between the two regions using the trajectory of the same Qdot-conjugated lipid. We analyzed three Qdot-conjugated lipids diffusing between GO and bare SiO_2 regions. The trajectory of each Qdot-conjugated lipid was fragmented at the point where it crossed the GO-SiO_2 boundary, and the fragmented trajectories on the GO and SiO_2 regions were analyzed separately. The diffusion coefficient at the GO region was lower than that at the SiO_2 region for all three Qdot-conjugated lipids (Figure 4-5b), and the values of *D* are summarized in Table IV-I. For example, *D* of Qdot 1 was 1.39 $\mu m^2/s$ in the GO region, which is ~70% of that in the bare SiO_2 region (1.99 $\mu m^2/s$). The value of *D* varies from 1.99 to 0.84 $\mu m^2/s$, even on the SiO_2

region, among the three Qdot-conjugated lipids (Table IV-I), probably because of the difference in the conjugation state such as multivalency. However, *D* was always lower in the GO region than the SiO_2 region, as seen from the comparison of the diffusion of the same Qdot. The cause of the slower diffusion in the SLB on GO will be the heterogeneous structure observed in Figure 4-3a. Domains in SLBs act as obstacles to lateral diffusion. It is known that the surface of GO consists of the nanoscale patches of the hydrophilic regions with oxygen functional groups and hydrophobic regions retaining pristine graphene structure.[29] The heterogeneity on the GO surface may be the cause of the domain formation in the SLB on GO, or it may perturb the assembly of lipids in the SLB, giving rise to a barrier for the lateral diffusion of lipids. The details of the relationship between the inner domain structures in SLB and the lateral lipid diffusion are subjects for future investigation.

Table IV-I. Diffusion coefficients of Qdot-conjugated lipids diffusing between the SLBs formed on the GO and SiO_2 regions.

	D_{GO} ($\mu m^2/s$)	D_{SiO2} ($\mu m^2/s$)	Ratio ($=D_{GO}/D_{SiO2}$) (%)
Qdot 1	1.39	1.99	69.9
Qdot 2	1.11	1.38	80.6
Qdot 3	0.45	0.84	53.9

4-4. Summary

We conjugated Qdots premodified with hetero-cross-linker and AEE to the SLB surface and performed SPT to evaluate the diffusion behavior of lipids in the SLB formed on GO. Diffusion of Qdot-conjugated lipid was observed in the SLB formed on GO and SiO_2, and we obtained sufficiently long trajectories of single Qdot-conjugated lipids for reliable analysis of mean-square displacement. The D-τ plot showed that the diffusion behavior of the

Qdot-conjugated lipid was normal random diffusion even in the SLB formed on GO. In addition, we found that the lipid diffusion was slower in the SLB on GO than in that on SiO_2 by comparing the diffusion coefficient of a single Qdot-conjugated lipid diffusing between the GO and SiO_2 regions. These results suggested that the properties and specific structure of the GO surface consisting of nanoscale hydrophilic and hydrophobic domains affected the lipid assembly of SLB, resulting in the lateral diffusion of lipids.

Reference

1) D. Lingwood and K. Simons, Science **327**, 46 (2010).

2) F. M. Ashcroft, Nature **440**, 440 (2006).

3) A. Hirano-Iwata, M. Niwano, and M. Sugawara, TrAC Trends Anal. Chem. **27**, 512 (2008).

4) E. T. Castellana and P. S. Cremer, Surf. Sci. Rep. **61**, 429 (2006).

5) M. Tanaka and E. Sackmann, Nature **437**, 656 (2005).

6) R. Tero, Materials **5**, 2658 (2012).

7) T. Hamada, M. Morita, M. Miyakawa, R. Sugimoto, A. Hatanaka, M. C. Vestergaard, and M. Takagi, J. Am. Chem. Soc. **134**, 13990 (2012).

8) R. Tero, Y. Suda, R. Kato, H. Tanoue, and H. Takikawa, Appl. Phys. Express **7**, 77001 (2014).

9) T. Isogai, A. Piednoir, E. Akada, Y. Akahoshi, R. Tero, S. Harada, T. Ujihara, and M. Tagawa, J. Cryst. Growth **401**, 494 (2014).

10) Y. Tamba, S. Ohba, M. Kubota, H. Yoshioka, H. Yoshioka, and M. Yamazaki, Biophys. J. **92**, 3178 (2007).

11) H. Nabika, Y. Inomata, E. Itoh, and K. Unoura, RSC Adv. **3**, 21271 (2013).

12) S. Ahmed, R. R. Madathingal, S. L. Wunder, Y. Chen, and G. Bothun, Soft Matter **7**, 1936 (2011).

13) K. Yamazaki, S. Kunii, and T. Ogino, J. Phys. Chem. C **117**, 18913 (2013).

14) Y. Shinozaki, K. Sumitomo, K. Furukawa, H. Miyashita, Y. Tamba, N. Kasai, H. Nakashima, and K. Torimitsu, Appl. Phys. Express **3**, 27002 (2010).

15) Y. Shinozaki, A. Tanaka, N. Kasai, K. Torimitsu, and K. Sumitomo, Appl. Phys. Express **7**, 27001 (2014).

16) A. Sumino, D. Yamamoto, M. Iwamoto, T. Dewa, and S. Oiki, J. Phys. Chem. Lett. **5**, 578 (2014).

17) A. Sumino, T. Dewa, T. Takeuchi, R. Sugiura, N. Sasaki, N. Misawa, R. Tero, T. Urisu, A. T. Gardiner, R. J. Cogdell, H. Hashimoto, and M. Nango, Biomacromolecules **12**, 2850 (2011).

18) M. S. Artiles, C. S. Rout, and T. S. Fisher, Adv. Drug Deliv. Rev. **63**, 1352 (2011).

19) X. Wang, C. Wang, K. Qu, Y. Song, J. Ren, D. Miyoshi, N. Sugimoto, and X. Qu, Adv. Funct. Mater. **20**, 3967 (2010).

20) K. P. Loh, Q. Bao, G. Eda, and M. Chhowalla, Nat. Chem. **2**, 1015 (2010).

21) A. Bonanni, A. H. Loo, and M. Pumera, TrAC Trends Anal. Chem. **37**, 12 (2012).

22) C.-H. Lu, H.-H. Yang, C.-L. Zhu, X. Chen, and G.-N. Chen, Angew. Chem. Int. Ed. Engl. **48**, 4785 (2009).

23) P. K. Ang, M. Jaiswal, C. H. Y. X. Lim, Y. Wang, J. Sankaran, A. Li, C. T. Lim, T. Wohland, O. Barbaros, and K. P. Loh, ACS Nano **4**, 7387 (2010).

24) S. Liu, T. H. Zeng, M. Hofmann, E. Burcombe, J. Wei, R. Jiang, J. Kong, and Y. Chen, ACS Nano **5**, 6971 (2011).

25) W. Gao, L. B. Alemany, L. Ci, and P. M. Ajayan, Nat. Chem. **1**, 403 (2009).

26) K. S. Novoselov, A. K. Geim, S. V Morozov, D. Jiang, M. I. Katsnelson, I. V Grigorieva, S. V Dubonos, and A. A. Firsov, Nature **438**, 197 (2005).

27) P. Avouris and C. Dimitrakopoulos, Mater. Today **15**, 86 (2012).

28) J. I. Paredes, S. Villar-Rodil, A. Martínez-Alonso, and J. M. D. Tascón, Langmuir **24**, 10560 (2008).

29) K. Erickson, R. Erni, Z. Lee, N. Alem, W. Gannett, and A. Zettl, Adv. Mater. **22**, 4467 (2010).

30) J. Kim, F. Kim, and J. Huang, Mater. Today **13**, 28 (2010).

31) K. Furukawa, Y. Ueno, E. Tamechika, and H. Hibino, J. Mater. Chem. B **1**, 1119 (2013).

32) R. Frost, G. E. Jönsson, D. Chakarov, S. Svedhem, and B. Kasemo, Nano Lett. **12**, 3356 (2012).

33) M. Hirtz, A. Oikonomou, T. Georgiou, H. Fuchs, and A. Vijayaraghavan, Nat. Commun. **4**, 1 (2013).

34) K. Tsuzuki, Y. Okamoto, S. Iwasa, R. Ishikawa, A. Sandhu, and R. Tero, J. Phys. Conf. Ser. **352**, 12016 (2012).

35) Y. Okamoto, K. Tsuzuki, S. Iwasa, R. Ishikawa, A. Sandhu, and R. Tero, J. Phys. Conf. Ser. **352**, 12017 (2012).

36) S. Mashaghi, T. Jadidi, G. Koenderink, and A. Mashaghi, Int. J. Mol. Sci. **14**, 4242 (2013).

37) W. S. Hummers and R. E. Offeman, J. Am. Chem. Soc. **80**, 1339 (1958).

38) R. Ishikawa, M. Bando, Y. Morimoto, S. Y. Park, and A. Sandhu, Jpn. J. Appl. Phys. **49**, 12 (2010).

39) R. Tero, T. Ujihara, and T. Urisu, Langmuir **24**, 11567 (2008).

40) R. Tero, H. Watanabe, and T. Urisu, Phys. Chem. Chem. Phys. **8**, 3885 (2006).

41) M. J. Murcia, D. E. Minner, G.-M. Mustata, K. Ritchie, and C. a Naumann, J. Am. Chem. Soc. **130**, 15054 (2008).

42) R. Tero, G. Sazaki, T. Ujihara, and T. Urisu, Langmuir **27**, 9662 (2011).

43) A. Kusumi, H. Ike, C. Nakada, K. Murase, and T. Fujiwara, Semin. Immunol. **17**, 3 (2005).

44) F. Daumas, N. Destainville, C. Millot, A. Lopez, D. Dean, and L. Salomé, Biophys. J.

84, 356 (2003).

45) T. Schmidt, G. J. Schütz, W. Baumgartner, H. J. Gruber, and H. Schindler, Proc. Natl. Acad. Sci. U. S. A. **93**, 2926 (1996).

Chapter 5

Effects of graphene oxide on morphology and lateral lipid mobility of lipid bilayers

Chapter 5. Effects of graphene oxide on morphology and lateral lipid mobility of lipid bilayers

5-1. Introduction

Lipid bilayers are a fundamental structure of plasma membranes, and plays important roles as a reaction field for various membrane reactions such as the transport of material, energy, and information into and out of cells.[1–3] The various artificial lipid membrane systems such as the black membrane, vesicle, and supported lipid bilayer (SLB) have been used extensively as the simply cell-membrane models to study the structure and physicochemical property of lipid bilayers. The SLBs formed at solid-liquid interfaces are more robust and stable than other artificial lipid membrane systems.[4–6] The SLBs are also valuable as a platform for investigating the function of membrane proteins, because the two-dimensional assembly and physical properties of lipids around the membrane proteins significantly affect the activity of the proteins.

Recently, graphene oxide (GO) with the unique physical and electronic properties was applied for the biological and biotechnological field. GO is the chemical derivative of graphene which is atomically two-dimensional sheet of sp^2-carbons, and is an excellent acceptor for fluorescence resonance energy transfer (FRET) over the entire visible wavelength region.[7–10] Therefore, GO was expected as the materials for FRET-based biosensors. In the theoretical calculation based on Förster mechanism the efficiency of fluorescence quenching by graphene is dependence to the minus forth power of the distance between donor molecule and GO[11]. Fluorescence lifetime measurement for eight DNA molecules with 6-carboxyfluorescein at the different position by J. Liu and co-workers[12] demonstrated that the quenching efficiency of GO was expressed as

$$Q = 1/[1+(d/d_0)^4] \quad (1),$$

where d was the distance between the GO and the DNA, and d_0 was the distance when the quenching efficiency was 50%.

In our previous work, we succeeded to form the SLB on GO-supported SiO_2/Si substrate by vesicle fusion method for the development of a new method to measure the molecular behavior in lipid membrane. The results of atomic force microscope (AFM) observation and fluorescence recovery after photobleaching (FRAP) measurement to SLB formed on GO/SiO_2/Si suggests that not only single SLB similar to hydrophilic oxide substrates, but also double SLBs were formed on GO. On the other hand, we estimated the fluidity of SLB on GO using the quantum dots (Qdots) as the fluorescence probe by the single particle tracking (SPT). The diffusion coefficient of Qdot-conjugated lipids at the GO region was lower than that at the SiO_2 region.

In the SLB system, its fluidity is maintained by a few nm layer of trapped water between the substrate and the bilayer. While, the physicochemical properties of SLB are affected by the interaction with the substrate because of the SLBs are located close to the substrate. Therefore, the investigation for the interaction between GO and lipid molecule into SLB is very important for the biological application of GO.

Herein, we estimated the interaction between the lipid molecule and the GO based on the dynamics of lipid molecule into SLB formed on GO by the SPT measurement. In the SPT measurement, we measured the fluorescence intensity of Qdot-conjugated lipid at the same time as acquiring the trajectory, evaluated the quenching efficiency of GO in SLB/GO systems. We used the SLB contained pegylated lipid to suppress the non-specific adsorption of Qdot to SLB surface for SPT measurement. We evaluated the effect of pegylated lipid for the structure and fluidity of SLB on GO.

5-2. Specific experimental condition

The vesicle suspension was prepared according the previous as mentioned method in Section 1, Chapter 2. The chloroform solution of dioleoylphosphatidylcholine (DOPC) was mixed with that of dioleoylphosphatidylethanolamine-N-(lissamine rhodamine B sulfonyl) (Rb-DOPE, E_x/E_m = 557/571 nm) as the fluorescence probe for FRAP, dipalmitoylphosphatidylthioethanol (DPPTE), and 1,2-distearoyl-sn-glycero-3-phosphoethanolamine-N-[amino(polyethylene glycol)-2000] (PEG-DSPE) at each molar ratio.

GO suspension was prepared according to the modified Hummer's method[13–15] as described in Chapters 2 and 3.

Each DOPC-SLB was prepared on the SiO_2/Si substrates with or without GO deposition by the vesicle fusion method[15–17] as mentioned in Section 2, Chapter 2. SLBs contained 2.5 – 7.5% of PEG-DSPE, 5×10^{-7}% of DPPTE for SPT, and additionally 0.2% of Rb-DOPE for FRAP measurement.

A carboxyl-coated Qdot (Lifetechnologies) was modified with a maleimide-hydrazide hetero-cross-linker (Quanta BioDesign) and 2-(2-aminoethoxy) ethanol (AEE) using 1-ethyl-3-(3-dimethylaminopropyl) carbodiimide (EDC), and then was added to a SLB containing DPPTE.[18] AEE was coadsorbed with the cross-linker to control the number of efficient maleimide groups on the Qdot surface for the covalent formation with DPPTE in the SLB, and to suppress the multivalent and/or non-specific adsorption of the Qdot.

The diffusion coefficient (*D*) was obtained based on the mean square displacement (MSD) analysis of the trajectories of dye-labeled lipid (Rb-DOPE) or Qdot-labeled lipid observed by SPT mentioned in Section 5, Chapter 2. Each fluorescence intensity was subtracted by the average fluorescence intensity of all frames to remove the effect of the back ground light and

the fluorescence by GO.

5-3. Results and discussion

We performed the single particle tracking to the DOPC-SLB containing 5% of PEG-DSPE formed on the GO/SiO_2/Si substrate after conjugating with Qdot. Figure 5-1 shows the fluorescence single particle image of Qdot-conjugated lipid and its trajectory in the SLB containing 5% of PEG-DSPE. The shape of the GO flakes were recognized because of the fluorescence from GO as shown in Chapter 4. We observed the Qdot-conjugated lipids on the GO region under the effect of the fluorescence quenching by GO. We found several Qdot-conjugated lipids diffused at both the GO region (the blue trajectory in Figure 5-1) and the SiO_2 region (the yellow trajectory in Figure 5-1).

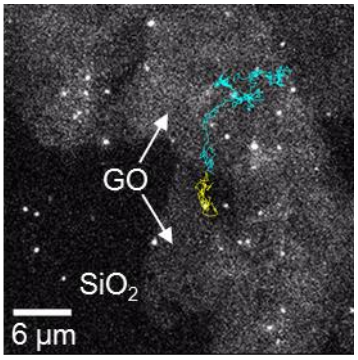

Figure 5-1. Fluorescence single particle image of Qdot-conjugated lipid in DOPC-SLB containing 5% of PEG-DSPE on the GO/SiO_2/Si substrate, and its trajectory on the GO region (blue) and on the SiO_2 region (yellow).

We evaluated the fluorescence quenching efficiency of GO by comparing the fluorescence intensity of Qdot at the GO region with that at the SiO_2 region. Figure 5-2 shows the fluorescence intensities obtained from six Qdot-conjugated lipids diffusing between the GO region and the SiO_2 region. The average fluorescence intensity at the GO region (F_{GO}) and that at the SiO_2 region (F_{SiO2}), the quenching efficiency of GO obtained from F_{GO} and F_{SiO2}, and

estimated distance between Qdot and GO were summarized in table V-I. The quenching efficiency (E) was estimated from following equation

$$E = 1 - F_{DA}/F_D = F_{GO}/F_{SiO2}, \qquad (2)$$

where F_{DA} and F_D are the fluorescence intensity of donor in presence of acceptor and in absence of acceptor, respectivity. The distance between Qdot and GO (d) was estimated from the quenching efficiency according to eq. (1).

The comparison of fluorescence intensities suggests that there were two groups of Qdots; those having F_{GO} clearly lower than F_{SiO2} (Qdot 1 (Figure 5-2a), Qdot 3(Figure 5-2c), Qdot 4 (Figure 5-2d), and Qdot 6 (Figure 5-2f)), and those with little difference between F_{GO} and F_{SiO2} (Qdot 2

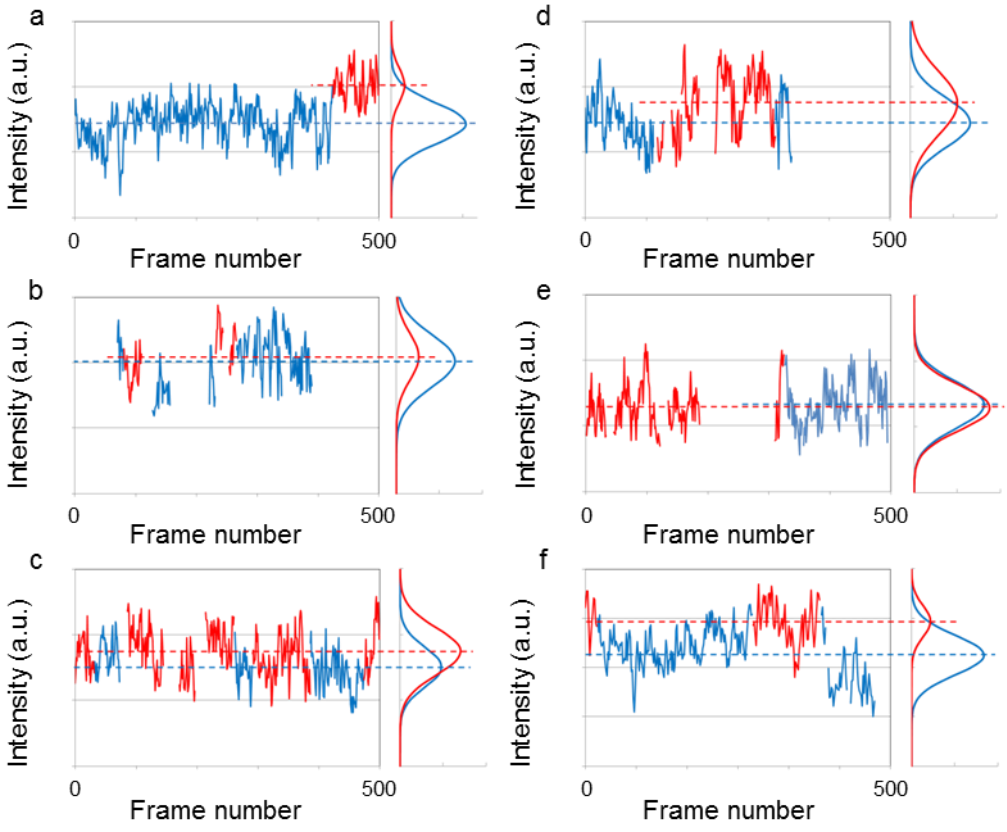

Figure 5-2. (a-f)Fluorescence intensity of Qdot conjugated with lipid molecule diffusing between the GO region (blue line) and the SiO_2 region (red line). Dotted lines are represented the average fluorescence intensity. The histograms of the fluorescence intensity in each region are illustrated on the right side of the graph.

(Figure 5-2b) and Qdot 5 (Figure 5-2e)). The quenching efficiencies of the former four Qdots which showed the large difference between the F_{GO} and F_{SiO2} were 0.29, 0.13, 0.19, and 0.23, respectively. On the other hands, the quenching efficiencies of the latter two Qdots (Qdot 2 and Qdot 5) were 0.03 and -0.03, respectively.

We presumed that the difference in quenching efficiency is due to the difference in distance between GO and Qdot. The curve in Figure 5-3 shows the relationship between the fluorescence quenching efficiency of GO and the distance from GO based on the equation (1). The estimated distances between the Qdots with higher quenching efficiency (Qdots 1, 3, 4, and 6) and GO were 9.4, 11.9, 10.9, and 10.1 nm, respectively. On the other hands, the estimated distance of Qdot 2 was 17.4 nm. Since the quenching efficiency of Qdot 5 was the negative value, the distance between Qdot and GO could not be estimated. The results were summarized in Table V-I. Qdot used in this study have cylindrical shape with the longer axis of 10 nm and the diameter of 5 nm approximately. The distance of ~10 nm obtained for the Qdots with higher

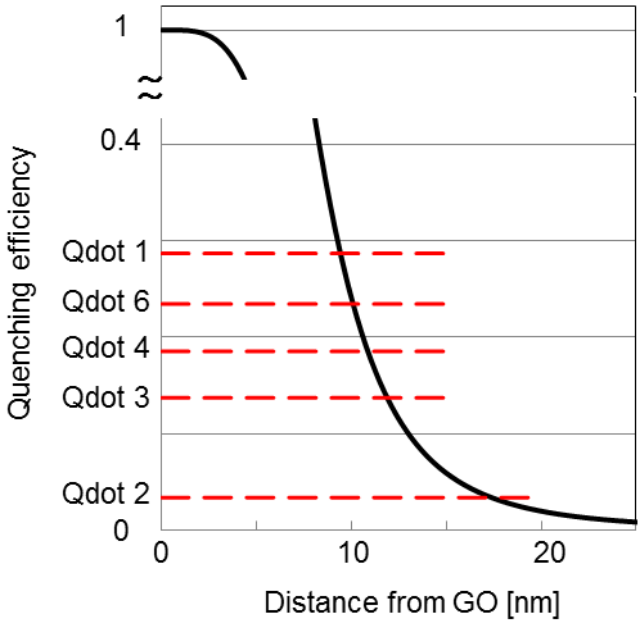

Figure 5-3. Fluorescence quenching efficiency versus distance plot of GO. Red dotted lines shows the estimated distance of each Qdot.

quenching efficiency is reasonable as a distance from GO to the center of Qdot existing on single SLB, if we consider the thickness of single lipid bilayer (~5 nm) and the size of the Qdot. As we described in Chapter 3, double SLB stacks on GO. It is reasonable that the other two Qdots with lower quenching efficiency existed on double SLBs where Qdots were hardly affected by the fluorescence quenching of GO, as shown Figure 5-3.

Table V-I. Fluorescence intensity of Qdots and estimated distance between Qdot and GO.

	F_{GO} [μm^2/s]	F_{SiO2} [μm^2/s]	Quenching efficiency	Estimated distance [nm]
Qdot 1	14.4	20.2	0.29	9.4
Qdot 2	20.2	20.9	0.03	17.4
Qdot 3	15.1	17.5	0.13	11.9
Qdot 4	14.5	17.8	0.19	10.9
Qdot 5	13.3	12.9	-0.03	-
Qdot 6	22.5	29.4	0.23	10.1

Qdots are used as donor fluorophores for various FRET-based biosensing.[19–23] In the FRET theory, the energy of an excited molecule is transferred by the dipole-dipole interaction between a donor and an acceptor. Despite Qdot is semi-conductor particle, it was reported that the energy of excited Qdots also transfer to the acceptor molecule and the efficiency of energy transfer depends on the minus six power of the distance between the Qdot center and the acceptor similarly to the case of a dye molecule as a donor.[23,24] The distance dependence in eq. (1) is derived for FRET between a dye molecule and GO, but we assume it is also valid for FRET Qdot and GO has validity.

We evaluated the fluidity of SLB containing 5% of PEG-DSPE on GO from the each trajectories of Qdot-conjugated lipid diffusing in the GO region and the SiO_2 region. We are able to evaluate the difference in fluidity between the SLBs on GO and on SiO_2, by comparing *D* between the two regions using the trajectory of the same Qdot-conjugated lipid. We analyzed

six Qdot-conjugated lipids diffusing between GO and bare SiO_2 regions. The trajectory of each Qdot-conjugated lipid was fragmented at the point where it crossed the GO-SiO_2 boundary, and the fragmented trajectories on the GO and SiO_2 regions were analyzed separately. Figure 5-4 shows the <MSD>-τ plots of six Qdot-conjugated lipids diffusing in the GO region and in the SiO_2 region. The *D* of Qdot-conjugated lipid at GO region obtained from <MSD>-τ plot was lower than that at the SiO_2 region for all six Qdot-conjugated lipids, and the values of *D* are summarized in Table V-II. The *D* values of these six Qdot-conjugated lipids were varied from 0.84 to 1.99 $\mu m^2/s$ even on the SiO_2 region. We estimated that these variations were caused by the difference in the number of lipids conjugated to quantum dots. We found that the diffusion of lipids in SLB on GO is always slower than that on SiO_2/Si substrate.

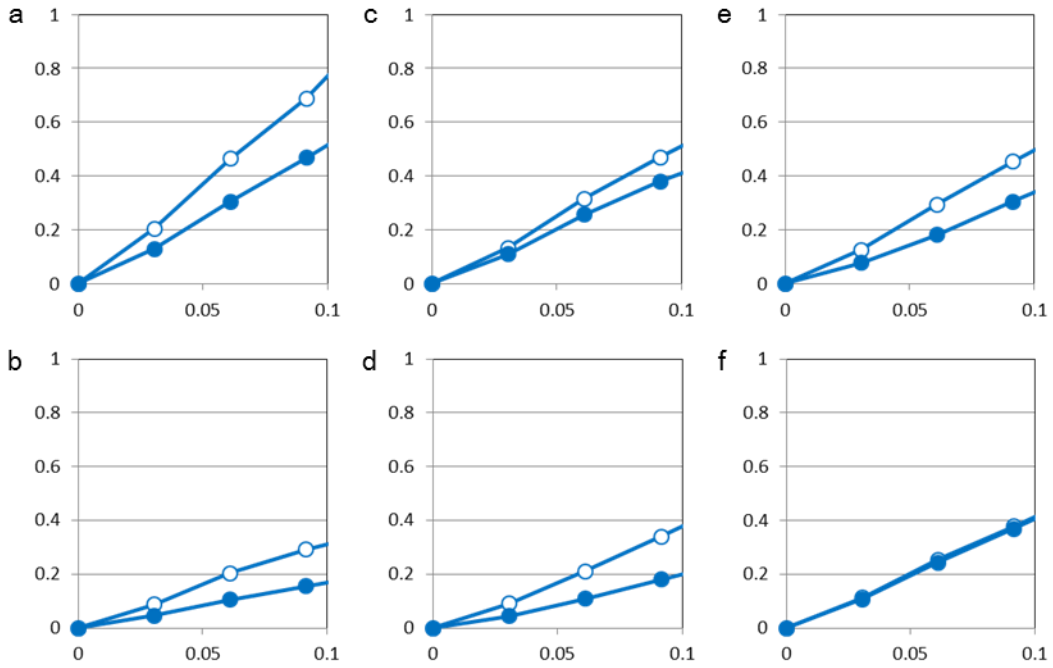

Figure 5-4. (a-f) <MSD>-τ plots of single Qdot-conjugated lipid diffusing on GO (filled circle) and on SiO_2 (blank circle).

Table V-II. Diffusion coefficients of Qdot-conjugated lipids diffusing between the SLBs formed on the GO and SiO_2 regions.

	D_{GO} [μm^2/s]	D_{SiO2} [μm^2/s]	Ratio (= D_{GO}/D_{SiO2}) [%]
Qdot 1	1.39	1.99	70
Qdot 2	1.11	1.38	81
Qdot 3	0.45	0.84	54
Qdot 4	0.72	1.01	71
Qdot 5	0.68	1.58	43
Qdot 6	0.87	1.10	79

We observed the morphology of the SLB containing 5% of PEG-DSPE by AFM. Figure 5-5 shows the AFM topography of SLB containing 5% of PEG-DSPE. We found that the SLB on the GO region was heterogeneous, while the SLB on the SiO_2/Si surface without GO was uniformly flat. Two regions with different heights were observed on the GO, and their heights from the SLB on SiO_2 were 6.36 and 3.23 nm, respectively. Both regions were higher than the SLB on SiO_2, therefore the two regions were attributed to domains in SLB with different thickness, not to a SLB and defects. According the structural model of the SLB on GO in Chapter 3, there is a possibility that not only single SLB but also double SLBs formed on GO. The height of the higher region was 6.36 nm, this value was reasonable when double SLBs were formed on GO. If single SLB was formed on GO, the height of first step from the SiO_2 region should be about 1.6 nm reflecting the height of the GO unless all PEG-DSPE aggregated on GO and the lipid composition was difference between the GO region and the SiO_2 region. However, the height of the lower region was 3.23 nm. These lower GO region were not a defect of SLB such as holes, because previous AFM studies show that the thickness of DOPC-SLB observed with tapping mode is 4-5 nm[25–28]. Therefore, we supposed that double SLBs were formed on the GO in common with the results of DOPC-SLB described in Chapter 3. The lipid domains

formed in SLB on GO were observed as a depression. The depth of the depression (lower) region was 2.73 nm, and the area fraction of the depression region (θ_{dep}) was 29.8% of the area of the GO region.

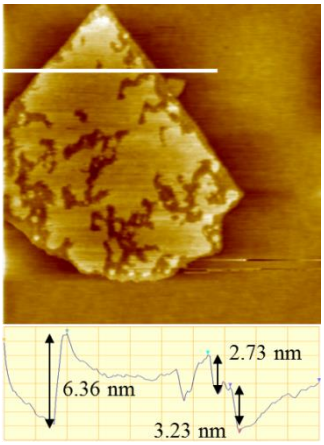

Figure 5-5. AFM topography of DOPC-SLB containing 5% of PEG-DSPE on the GO/SiO_2/Si substrate and its cross-section profile at the white line. Image size was 3 μm×3

We observed the SLB containing PEG-DSPE at 2.5%, 5.0% and 7.5% molar ratio formed on the bare SiO_2/Si substrate without GO. S. Kaufmann et al. reported that the diffusion coefficient of POPC-SLB containing 8 mol% PEG-DOPE was decreased substantially and no recovery was seen in POPC-SLB containing 10 mol% PEG-DOPE[29]. In order to maintain the fluidity of SLB, we experimented by using the SLB containing PEG-DSPE less than the concentration of 8%. Figure 5-6a, 5-6b and 5-6c show the AFM topographies of the SLB containing 2.5%, 5.0% and 7.5% of PEG-DSPE, respectively. In the SLB containing 2.5% of PEG-DSPE (Figure 5-6a), the SLB surface was almost uniform and we rarely found a depression region (θ_{dep} ~0.1%). In SLB containing 5% of PEG-DSPE (Figure 5-6b), we found that several depressions existed, and the θ_{dep} was 0.3%. The area fraction of the depression increased to 17.9% in the SLB containing 7.5% of PEG-DSPE (Figure 5-6c). These results indicate that the depression domain was the PEG-DSPE-rich domain, because dep increased with the concentration of PEG-DSPE.

It seems strange that the “depressed” region increased when the amount of a lipid with a

bulky PEG chain. We should note that what AFM topography is mapping of constant-force point between a probe and a sample, not always the actual geometry of the sample surface. According to the recent study by Kauffman et al.,[29] the AFM force-distance curve shows that the distance decreased with the concentration of pegylated lipid at loading force higher than ~1 nN. This report supports that a domain containing more PEG-DSPE is possibly observed lower than a region with less PEG-DSPE. Hydrophilic polymer chain caused steric forces, which strongly depends on the conformation and fluctuation of the polymer chain. The conformation of PEG chains is affected by the distance between neighboring PEG chains.[30,31] PEG chains take the mushroom-like conformation at low PEG density. The PEG-DSPE freely diffuses and fluctuates in the fluid SLB in the liquid crystalline phase. The appearance of the domains at the PEG-DSPE concentration higher than 5% indicates the PEG-DSPE aggregates and restricts the movement of PEG-DSPE. The height of the depression domain obtained by AFM was observed lower than the surrounding region because of the hydration repulsive force and steric repulsion between the probe and PEG chain was decreased due to suppress the fluctuation by the aggregation of PEG chains.

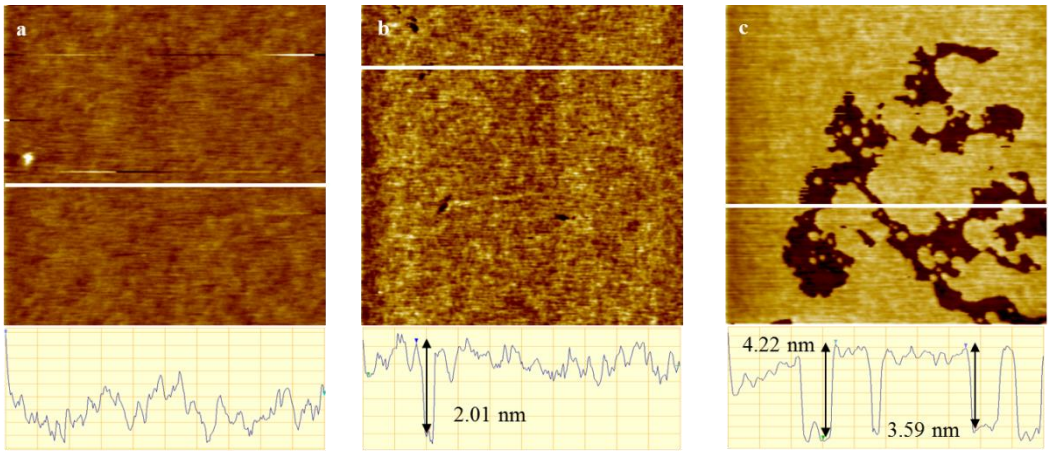

Figure 5-6. AFM topographies of DOPC-SLB containing (a) 2.5%, (b) 5.0%, and (c) 7.5% of PEG-DSPE on bare SiO_2/Si substrate and its cross-section profile at white line. Image sizes are (a) 1.0 μm×1.0 μm, (b) 2.0 μm×2.0 μm, and (c)10 μm×10 μm.

We found an effect of localizing the specific lipid domain on GO. We assumed that this phenomenon is due to the heterogeneous surface of GO, which has hydrophilic oxidized region and hydrophobic graphene domain in nanoscale. This hydrophobic graphene domain in GO surface had high surface energy in water and behaved as an active site. Pegylated lipids diffusing from the surrounding area were trapped on the hydrophobic graphene sites, and became the nucleus to form the lipid domain. Alternatively, since vesicles containing pegylated lipids preferentially adsorbed on the hydrophobic graphene site and transformed to SLB, pegylated lipids-rich domain was existed only on GO.

We evaluated the *D* of SLB containing PEG-DSPE at each molar ratio formed on bare SiO_2/Si by the FRAP measurement with a laser scanning fluorescence microscope. We obtained the *D* by fitting to the recovery rate of square area after photobleaching on the basis of the theory and protocol reported by Berquand.[32] Figure 5-7 shows the recovery curve after photobleaching of SLB containing PEG-DSPE at each molar ratio. *D* values of SLB containing PEG-DSPE at each molar ratio were 2.84 ± 0.21 (n=5) (2.5% of PEG-DSPE in Figure 5-7a), 2.50 ± 0.53 (n=5) (5.0% of PEG-DSPE in Figure 5-7b), and 0.76 ± 0.18 (n=6) (7.5% of PEG-DSPE in Figure 5-7c) $\mu m^2/s$, respectively. *D* values were decreased with the concentration of PEG-DSPE. FRAP measurement indicated the correlation between the *D* and the concentration of PEG-DSPE. Because there was also the correlation between the θ_{dep} and the concentration of PEG-DSPE, we conclude that the *D* was decreased by the increase of PEG-DSPE-rich domain due to increase the concentration of PEG-DSPE.

The results of AFM observation (Figure 5-6) and FRAP measurement (Figure 5-7) show that the θ_{dep} increased and *D* decreased with the concentration of PEG-DSPE in DOPC-SLB. Therefore the reason why the *D* of SLB on GO was decreased (Table V-II) is the localization of

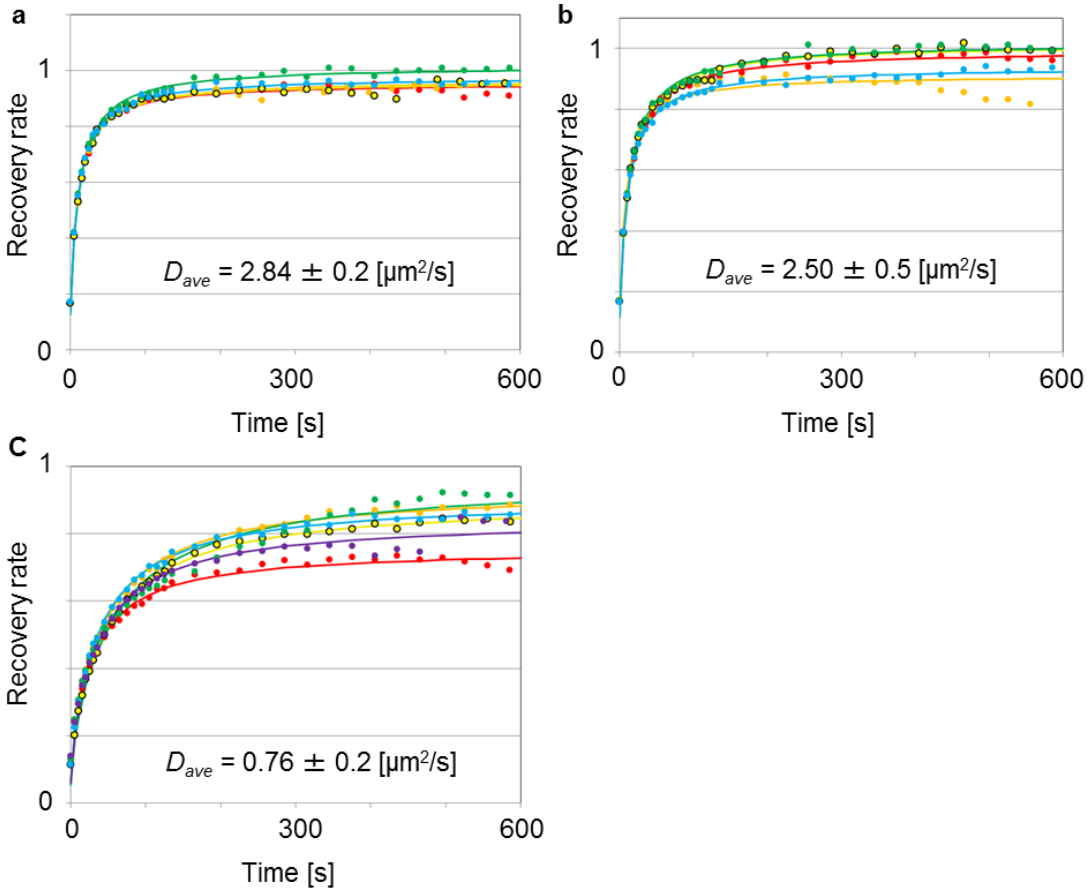

Figure 5-7. Recovery curve of SLB containing (a)2.5%, (b)5.0%, and (c)7.5% of PEG-DSPE on the bare SiO_2/Si substrate in FRAP measurement. Filled circles show the recovery rate and the line of the same color as the circle shows the fitting curve.

the PEG-DSPE-rich depression domain on GO (Figure 5-5). Since the θ_{dep} on GO was 29.8%, it was predicted that the concentration of PEG-DSPE in SLB on GO was higher than that in SLB containing 7.5% of PEG-DSPE on bare SiO_2/Si substrate, which θ_{dep} is 17.9%. However, the rate of decrease of *D* by the effect of PEG-DSPE-rich domains in SLB on GO was smaller than that on bare SiO_2/Si substrate. We suppose that this difference of decrease rate of *D* attributed to the measurement method. In the SPT measurement on the basis of the diffusion behavior of single molecule, the *D* reflected the molecule behavior in the SLB on GO other than the PEG-DSPE-rich domain because of the diffusion barrier at the domain boundary. While, the *D* obtained by FRAP measurement was the mean value of the diffusion behavior of lipids in the

macroscopic domain, which included the lipids diffusing across the lipid domain and within the lipid domain.

We expect that the effect of localizing the specific lipid domain of GO controls the position at which the membrane proteins are reconstructed. Furthermore, it is easy to regularly arrange GO on the substrate, and it becomes possible to reconstruct the membrane proteins to the arranged SLB/GO systems. The SLB/GO system will be able to apply to a microarray system for the investigation of membrane proteins.

5-4. Summary

We evaluated the quenching efficiency by GO and the diffusion behavior of lipids in SLB on GO by the SPT measurement using Qdots as a fluorescence probe. Diffusion of Qdot-conjugated lipid was observed in the SLB formed on GO and SiO_2, and we obtained the fluorescence intensity of Qdot at both the GO region and the SiO_2 region. We estimated the Qdot-GO distance from the quenching efficiency based on FRET theory. We obtained sufficiently long trajectories of single Qdot-conjugated lipids for reliable analysis of mean-square displacement. We found that the lipid diffusion was slower in the SLB on GO than in that on SiO_2 by comparing the diffusion coefficient of a single Qdot-conjugated lipid diffusing between the GO and SiO_2 regions. We clarified that the reason for the decrease in D of SLB on GO is due to the localization of PEG-DSPE on GO by AFM observation. These results suggested that the properties and specific structure of the GO surface consisting of nanoscale hydrophilic and hydrophobic domains trapped more rigid lipids in promoted affected the lipid assembly of SLB, resulting in the lateral diffusion of lipids.

Reference

1) D. Lingwood and K. Simons, Science **327**, 46 (2010).

2) F. M. Ashcroft, Nature **440**, 440 (2006).

3) A. Hirano-Iwata, M. Niwano, and M. Sugawara, TrAC Trends Anal. Chem. **27**, 512 (2008).

4) E. T. Castellana and P. S. Cremer, Surf. Sci. Rep. **61**, 429 (2006).

5) M. Tanaka and E. Sackmann, Nature **437**, 656 (2005).

6) R. Tero, Materials **5**, 2658 (2012).

7) J. Kim, F. Kim, and J. Huang, Mater. Today **13**, 28 (2010).

8) J.-L. Li, H.-C. Bao, X.-L. Hou, L. Sun, X.-G. Wang, and M. Gu, Angew. Chem. Int. Ed. Engl. **51**, 1830 (2012).

9) K. P. Loh, Q. Bao, G. Eda, and M. Chhowalla, Nat. Chem. **2**, 1015 (2010).

10) E. Morales-Narváez and A. Merkoçi, Adv. Mater. **24**, 3298 (2012).

11) R. S. Swathi and K. L. Sebastian, J. Chem. Phys. **129**, 54703 (2008).

12) M. Wu, R. Kempaiah, P.-J. J. Huang, V. Maheshwari, and J. Liu, Langmuir **4**, 2731 (2011).

13) W. S. Hummers and R. E. Offeman, J. Am. Chem. Soc. **80**, 1339 (1958).

14) R. Ishikawa, M. Bando, Y. Morimoto, S. Y. Park, and A. Sandhu, Jpn. J. Appl. Phys. **49**, 12 (2010).

15) Y. Okamoto, K. Tsuzuki, S. Iwasa, R. Ishikawa, A. Sandhu, and R. Tero, J. Phys. Conf. Ser. **352**, 12017 (2012).

16) R. Tero, T. Ujihara, and T. Urisu, Langmuir **24**, 11567 (2008).

17) R. Tero, H. Watanabe, and T. Urisu, Phys. Chem. Chem. Phys. **8**, 3885 (2006).

18) M. J. Murcia, D. E. Minner, G.-M. Mustata, K. Ritchie, and C. a Naumann, J. Am. Chem. Soc. **130**, 15054 (2008).

19) K. E. Sapsford, L. Berti, and I. L. Medintz, Angew. Chemie - Int. Ed. **45**, 4562 (2006).

20) K. D. Wegner and N. Hildebrandt, Chem. Soc. Rev. (2015).

21) I. L. Medintz and H. Mattoussi, Phys. Chem. Chem. Phys. **11**, 17 (2009).

22) U. Resch-Genger, M. Grabolle, S. Cavaliere-Jaricot, R. Nitschke, and T. Nann, Nat. Methods **5**, 763 (2008).

23) I. L. Medintz, H. T. Uyeda, E. R. Goldman, and H. Mattoussi, Nat. Mater. **4**, 435 (2005).

24) D. M. Willard, L. L. Carillo, J. Jung, and A. Van Orden, Nano Lett. (2001).

25) E. I. Goksu, B. A. Nellis, W.-C. Lin, J. H. Satcher, J. T. Groves, S. H. Risbud, and M. L. Longo, Langmuir **25**, 3713 (2009).

26) J. T. Marquês, A. S. Viana, and R. F. M. De Almeida, Biochim. Biophys. Acta **1808**, 405 (2011).

27) P.-E. Milhiet, F. Gubellini, A. Berquand, P. Dosset, J.-L. Rigaud, C. Le Grimellec, and D. Lévy, Biophys. J. **91**, 3268 (2006).

28) F. Domenici, D. Panichelli, and A. C. Castellano, Colloids Surf. B. Biointerfaces **69**, 216 (2009).

29) S. Kaufmann, O. Borisov, M. Textor, and E. Reimhult, Soft Matter **7**, 9267 (2011).

30) O. Tirosh, Y. Barenholz, J. Katzhendler, and A. Priev, Biophys. J. **74**, 1371 (1998).

31) A. Vonarbourg, C. Passirani, P. Saulnier, and J. P. Benoit, Biomaterials **27**, 4356 (2006).

32) A. Berquand, P. E. Mazeran, J. Pantigny, V. Proux-Delrouyre, J. M. Laval, and C. Bourdillon, Langmuir **19**, 1700 (2003).

Chapter 6

Physicochemical properties of lipid bilayer consisting of partially fluorinated phospholipid

Chapter 6. Physicochemical properties of lipid bilayer consisting of partially fluorinated phospholipid

6-1. Introduction

The lipid bilayer is the fundamental structure of biomembranes such as a plasma membrane and subcellular organelles, and plays crucial roles in the transportation of signals and materials through the functions of membrane proteins and the organization of lipid domains.[1)] Membrane proteins retain their specific structures owing to the environments provided by the surrounding lipid molecules.[2,3)] Hydrophobic interaction via the fluidity, thickness and direct molecular coordination at the hydrophobic core in lipid bilayers is one of dominant factors for membrane proteins to exert the proper structures and biological functions.[3–8)] Control of intermolecular interaction in the hydrophobic region of lipid bilayer membranes is demanded for the extraction and reconstruction of membrane proteins *in vitro*. Fluorinated lipids and surfactants are expected for biological applications such as surface modification for biomimetic materials, drug delivery systems, extraction and reorganization of membrane proteins, because of their biological inertness and chemical stability.[9–16)] Frotscher et al. reported a superior performance of the fluorinated octylmaltoside derivative F_6OM in chaperoning the functional refolding of an integral membrane enzyme, because its mild and unusual mode of detergency promotes bilayer insertion.[12)] However many points about the mechanism of molecular interaction fluorinated lipids and surfactants are still not clear.[15,17)] It is necessary to evaluate fundamental physical properties of assembled structures fluorinated lipids and surfactants experimentally to understand details of the mechanism.

Recently, Sonoyama and co-workers synthesized a novel partially fluorinated lipid,

1,2-di-(11,11,12,12,13,13,14,14,14-nonafluorotetradecanoyl)-sn-glycero-3-phosphocholine (F4-DMPC, which was expressed as diF4H10 in the literatures[18–20]), an analog of a common 1,2-dimyristoyl-sn-glycero-3-phosphocholine (DMPC) with the perfluorinated butyl segment in the myristoyl group, and investigated its thermal and interfacial properties.[19,21] Differential scanning calorimetry (DSC) measurement of the mixture of F4-DMPC and DMPC indicates that the interaction between F4-DMPC and DMPC cannot be simply interpreted only in terms of the separation between fluorocarbons and hydrocarbons.[19] They also revealed that the bacteriorhodopsin reconstructed in the vesicle of F4-DMPC retains a native-like structure, photocycles and a stability against the visible light irradiation.[20] These results strongly suggest that the F4-DMPC affects lipids and membrane proteins in a different manner from the common phospholipids with hydrocarbon chains.

In this study, we investigated the intermolecular interaction of the partially fluorinated lipid in a bilayer membrane, which was derived from the area thermal expansion coefficient, lateral lipid mobility and its temperature dependence. The apparent activation energy of lateral lipid diffusion (E'_a) is a fundamental indicator for the lipid-lipid and lipid-protein intermolecular interaction in lipid bilayer membranes.[22–24] The diffusion coefficients of the supported lipid bilayer (SLB) of F4-DMPC were measured by the single particle tracking (SPT) method, and compared with 1,2-dioleoyl-sn-glycero-3-phosphocholine (DOPC)-SLB as a control. We quantitatively evaluated the effect of the fluorocarbon segments on the intermolecular interaction in the hydrophobic region of the lipid bilayer.

6-2. Specific experimental condition

F4-DMPC was synthesized using the same protocol as in the previous literature.[21] The vesicle

suspensions of F4-DMPC and DOPC were prepared by previously mentioned in Section 1, Chapter 2. The chloroform was dried in a glass tube with a N_2 stream, followed by an over-night vacuum pumping in a desiccator. The molar ratio of 1,2-dioleoyl-sn-glycero-3-phospho-ethanolamine-N-(lissamine rhodamine B sulfonyl) (Rb-DOPE, Ex 557 nm / Em 571 nm) as a fluorescence probe to F4-DMPC or DOPC was 0.2% for the observation with epi-fluorescence microscope, and 1×10^{-6}% for SPT. We prepared the vesicle suspension of F4-DMPC and DOPC according the previous mentioned manner in Chapter 2.

We observed the SLBs of F4-DMPC and DOPC and performed fluorescence recovery after photobleaching (FRAP) for qualitative evaluation of the membrane fluidity with an epi-fluorescence microscope (Olympus BX51W) equipped with a 60× water-immersion lens. The sample temperature was changed at a cooling rate of 1 °C per minute, and held for 10 minutes at each temperature before observation. We evaluated the coverage of the SLB from the fluorescence images by using ImageJ, as the average of six to eight images obtained at different position of the sample.

The diffusion coefficient (D) was obtained by a mean square displacement (MSD) analysis of the diffusion trajectories of dye-labeled lipid (Rb-DOPE), which was observed by SPT.[25–28] We obtained the trajectory coordinates from the movies using ImageJ on the basis of the theory and protocol developed by Sbalzarini and Koumoutsakos.[29] Detailed information was mentioned in Section 5, Chapter 2.

Prior studies showed that the temperature dependence of D of a lipid molecule in a homogeneous lipid bilayer membrane is expressed on the basis of the free-volume theory.[22–24] Detail information was mentioned in Section 6, Chapter 2.

Standard error of gradient (S_a) was calculated as

$$S_a = \sqrt{\sum \left(y - y_{average}\right)^2 \Big/ (n-2) \sum \left(x - x_{average}\right)^2}$$

for linear fitting of $y = ax + b$. Note that S_a is different from a standard deviation among a group of isolated data points and depends on the range of x (=1/T in eq. (4), on the order of 10^{-4} in this study).

Equations (2) and (4) show that the interaction term E'_a is extracted from the gradient of the Arrhenius plot, while D is also affected by the term of A_0 which relates to molecular size. The activation energy E_a (eq. (3)) in a lipid bilayer takes into account the molecular interaction between neighboring molecules, the energy required to create a vacancy next to the diffusing molecule, and also the interaction with the surrounding aqueous media.[22] Additionally in SLB systems, underlying solid substrates should be concerned.[30–32] Therefore we are able to evaluate the difference in the intermolecular interaction between two SLBs with different components from E'_a and α, on the condition that the lipid head groups, aqueous media and solid substrates are the same. Typical values of E'_a of non-fluorinated phosphatidylcholines (PCs) are 25 − 45 kJ/mol[33,34]. Unsaturated PCs including DOPC in giant unilamellar vesicles (GUVs) and multilamellar systems have α of 1.3×10^{-3} K^{-1} to 3×10^{-3} K^{-1},[33,35–40] and they are nearly independent of temperature at 15 - 40 °C, sufficiently above their phase transition temperature (T_c) between the gel and liquid crystalline phases.[39,40] On the other hand the α of saturated PC, e.g. DMPC (non-fluorinated), highly depends on temperature near T_c (24 °C for DMPC):[36,41,42] α=$10.1 \pm 0.5 \times 10^{-3}$ K^{-1} at 25 °C, $4.2 \pm 0.2 \times 10^{-3}$ K^{-1} at 35°C in ref. [41]. In eq. (3), α is assumed to be independent of T at the temperature range of interest. Therefore DOPC is suitable as a control in this study, rather than DMPC.

6-3. Results and discussion

Figure 6-1a is a typical fluorescence image of F4-DMPC-SLB observed at 24 ˚C. A

homogeneous SLB was formed on the SiO_2/Si substrate with an average coverage (θ) of 0.959. Defects were observed as dark regions of a few micrometers. First we verified whether the solid-supported bilayer system in the present study was available to investigate the basic physical properties of F4-DMPC bilayer. The lateral molecular diffusion and phase transition are generally retained in SLB systems, but artificial phase transition phenomena, e.g. shift of T_c and decoupled phase transition, may appear in the condition of a strong substrate-SLB interaction.[30–32] Figures 6-1b, 6-1c, and 6-1d show the fluorescence image sequence of F4-DMPC-SLB during the FRAP process. Temporal recovery of the fluorescence intensity at the bleached region revealed that F4-DMPC-SLB was fluid at 24 ˚C. We performed FRAP at various temperatures lower than 24 ˚C, and found that the lateral lipid diffusion was hindered at 2 ˚C (Figure 6-2), while F4-DMPC-SLB was fluid above 5 ˚C. This result is in good agreement with the previous study using DSC and X-ray diffraction: The multilamellar vesicle of F4-DMPC has its main endothermic peak at 5.4 ˚C in the DSC curve, and two peaks in the X-ray diffraction pattern disappeared above 5 ˚C.[21] The FRAP results in this study (Figure 6-1 and Figure 6-2) confirmed that the main transition in the DSC experiment is that between the

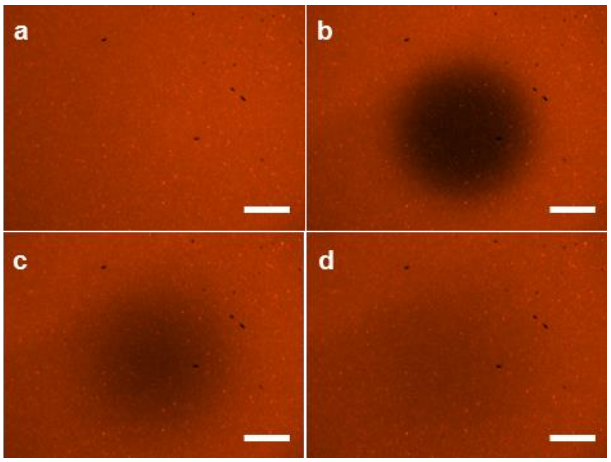

Figure 6-1. Fluorescence images of the F4-DMPC-SLB and the FRAP process obtained at 24 ˚C. (a) Before photobleaching. (b) 0 s, (c) 60 s, and (d) 180 s after the photobleaching. Scale bars correspond to 20 μm.

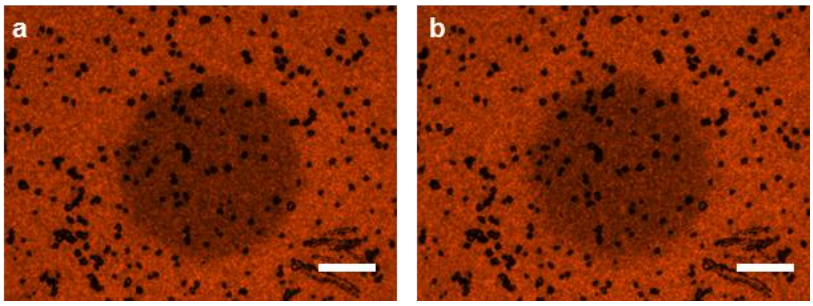

Figure 6-2. Fluorescence images of F4-DMPC-SLB at 2 ˚C acquired (a) 0 s and (b) 276 s after photobleaching. The photobleaching was performed for 15 s by the irradiation of the excitation light 278 times brighter than that for observation. Scale bars correspond to 20 μm.

gel (solid) and liquid crystalline (L_α) (fluid) phases, and that the transition behavior of F4-DMPC is retained in the SLB system.

We estimated the area thermal expansion coefficient (α) of F4-DMPC-SLB, because it represents disorderliness and the thermal fluctuation of hydrophobic tails and hence relates to the apparent activation energy of diffusion (eq. (3)).[22,23] Figure 6-3 shows the temperature dependence of θ of F4-DMPC-SLB obtained from the fluorescence images. The typical fluorescence images observed at each temperature are shown in Figure 6-4. The average θ values of F4-DMPC-SLB were reduced from 0.959 to 0.932 with a decrease of temperature at

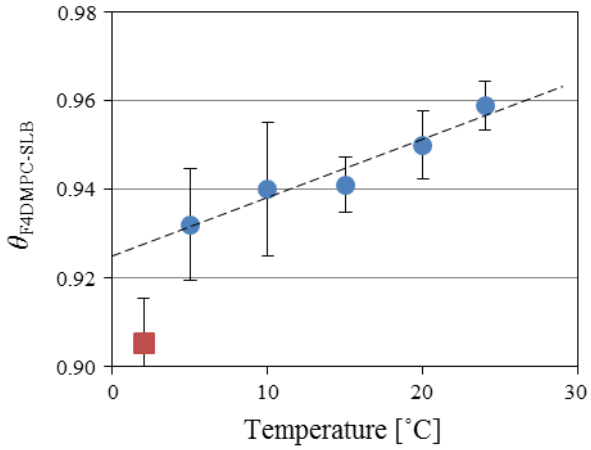

Figure 6-3. Dependence of the coverage (θ) of F4-DMPC-SLB on temperature. Blue circles and a red square represent that F4-DMPC-SLB was in the L_α (fluid) phase (5 to 24 ˚C) and gel (solid) phase (2 ˚C), respectively

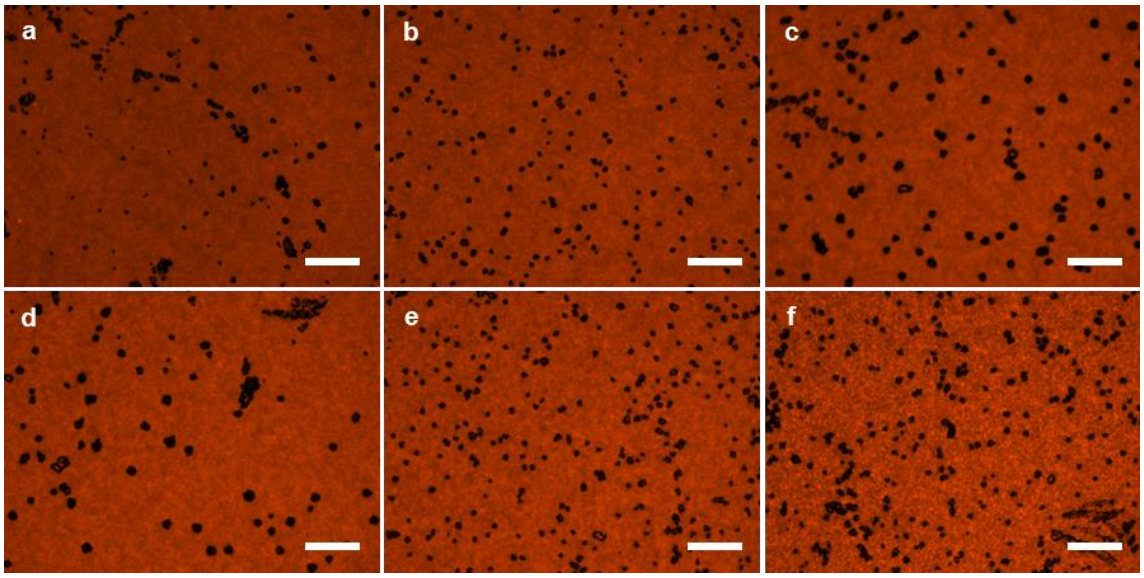

Figure 6-4. Typical fluorescence images of F4-DMPC-SLB at (a) 24 ˚C (θ = 0.959±0.006, *n*=7), (b) 20 ˚C (θ = 0.950±0.008, *n*=7), (c) 15 ˚C (θ = 0.941±0.006, *n*=8), (d) 10 ˚C (θ = 0.940±0.015, *n*=8), (e) 5 ˚C (θ = 0.932±0.013, *n*=8), and (f) 2 ˚C (θ = 0.905±0.010, *n*=6). Scale bars correspond to 20 μm.

24 to 5 ˚C because of thermal shrinkage. We observed a discrete shrinkage from 5 to 2˚C (θ = 0.905). This temperature region corresponds to the L_α–gel phase transition temperature in the FRAP experiments (Figure 6-1 and Figure 6-2) and in the previous DSC and X-ray diffraction results as described above.[19,21] The result also supports the L_α-gel transition of F4-DMPC, because the discrete reduction in area due to the L_α-gel phase transition is a common property in lipid bilayers.[22,23] We obtained $\alpha = (1/\theta)(\Delta\theta/\Delta T)$ to be 1.4 ± 0.17 × 10^{-3} K^{-1} for F4-DMPC-SLB from the slope of the linear fitting between 24 ˚C and 5 ˚C in Figure 6-3, assuming that the temperature dependence of θ was linear in the narrow temperature range of Figure 6-3. The α value of F4-DMPC-SLB was nearly independent of temperature even near T_c. It is a substantial difference from non-fluorinated PCs: DMPC (non-fluorinated) shows "anomalous" temperature dependence in α in ~10 ˚C region above T_c because of subcritical fluctuation.[36,41,42] From the view point of area thermal expansion, F4-DMPC just above T_c behaves similarly to unsaturated PCs sufficiently above their T_c (e.g. −17 ˚C for DOPC).

We performed SPT to obtain *D* of F4-DMPC-SLB and its temperature dependence. In this study SPT was appropriated rather than FRAP, because defects existed in F4-DMPC-SLB and increased its area with the reduction of temperature (Figure 6-3 and Figure 6-4). Figures 6-5a and 6-5b show the fluorescence intensity distribution and the snapshots of a single molecule fluorescence image of Rb-DOPE in the F4-DMPC-SLB a SPT movie, respectively. Sufficient signal to noise ratio was obtained to track the diffusion of Rb-DOPE molecules in F4-DMPC-SLB. The typical trajectories of Rb-DOPE obtained at 25 ˚C, 20 ˚C, and 15 ˚C are shown in Figure6-5c. The diffusion distances were diminished with decreasing the temperature. We evaluated *D* by the MSD analysis of the trajectories.

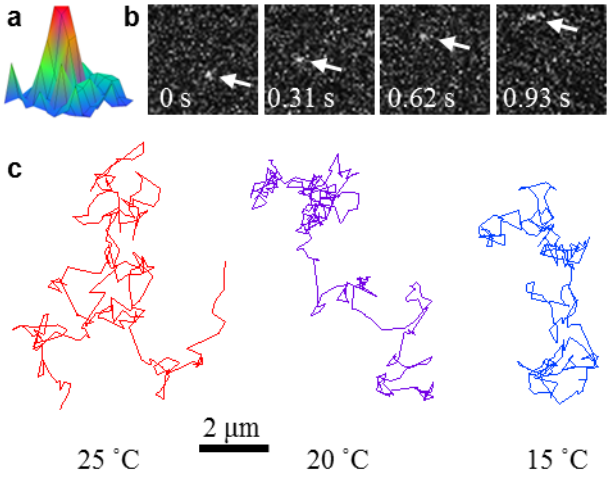

Figure 6-5. (a) Fluorescence intensity distribution from a single Rb-DOPE molecule in F4-DMPC-SLB obtained from a single frame of a SPT movie. (b) Captured snapshots (9 μm × 9 μm) of a Rb-DOPE molecule diffusing in F4-DMPC-SLB at 15 ˚C, taken at every 20 frames (0. 31 s). (c) Trajectories of Rb-DOPE at 25, 20, and 15 ˚C. The elapsed times of the trajectories are 3.9 s (255 frames), 4.7 s (304 frames), and 3.8 s (245 frames), respectively.

Figure 6-6a shows the ⟨MSD⟩ of the trajectories of Rb-DOPE in F4-DMPC-SLB at 25 ˚C, 20 ˚C, and 15 ˚C plotted against τ. The MSD-τ plots of all trajectories used for the calculation of ⟨MSD⟩ at each temperature are shown in Figure 6-7. In Figure 6-6a, ⟨MSD⟩ showed linear dependence on τ at all the temperatures, and the gradient of the ⟨MSD⟩-τ plot had a tendency to

decrease with temperature. The *D* values obtained from the linear fitting of ⟨MSD⟩ until τ = 1.0 s according to eq. (1) for each ⟨MSD⟩-τ plot were 1.90 μm^2/s at 25 ˚C, 1.51 μm^2/s at 20 ˚C, and 1.18 μm^2/s at 15 ˚C.

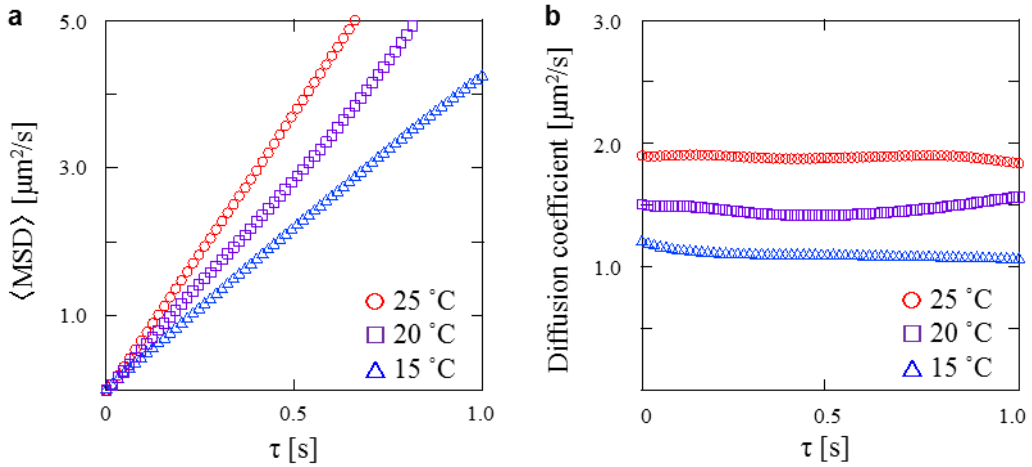

Figure 6-6. (a) ⟨MSD⟩ versus τ plots and (b) diffusion coefficient (*D*) versus τ plots at 25 ˚C (red circles), 20 ˚C (purple squares), and 15 ˚C (blue triangles).

Figure 6-6b shows the tendency of *D* on τ at each temperature. It provides information about spatiotemporal diffusion behavior such as a normal diffusion or an anomalous diffusion.[28,43,44] In the case of anomalous diffusion, *D* changes with τ because of the interaction between the probe molecule and heterogeneous environments such as corrals or obstacles. The *D* versus τ plot in Figure 4b shows that the *D* was almost independent of τ within the region of the diffusion distance until τ = 1 s. The average diffusion distance, $\sqrt{\langle MSD \rangle} = \sqrt{\langle 4D\tau \rangle}$, at τ = 1.0 s was 2.8 μm at 25 ˚C, and 2.2 μm at 15 ˚C. We conclude that the F4-DMPC-SLB was homogeneous at least at a range of ~3 μm at the temperatures in this study. This distance was sufficiently short compared to the distance between the defects observed in Figures 6-1 and 6-4. Therefore, the effect of defects was negligible for the evaluation of *D* by the SPT measurement on the spatiotemporal scale in this study. In general, the FRAP method provides the average diffusion rate over a region of several tens of micrometers,[45–47] and is also affected by the

obstacles outside the photobleached region. The SPT measurement was suitable to evaluate the fluidity of F4-DMPC-SLB accurately.

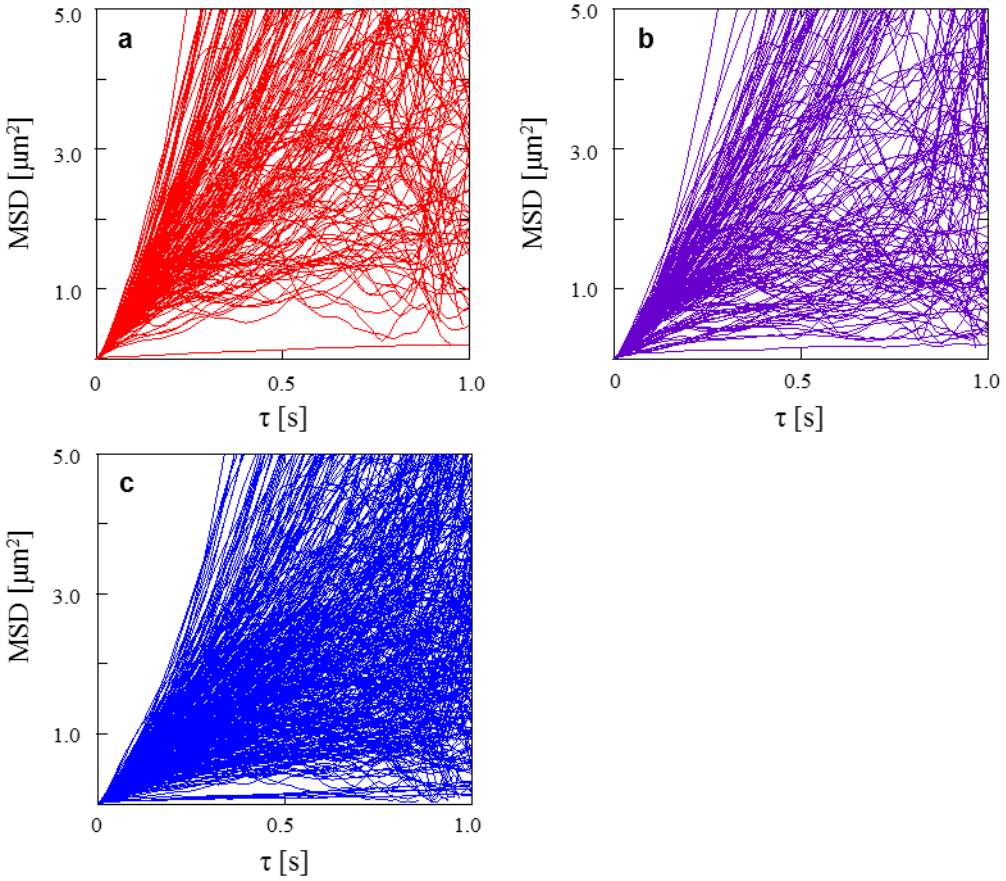

Figure 6-7. MSD versus τ plots of all trajectories obtained for F4-DMPC-SLB at (a) 25 ˚C, (b) 20 ˚C, and (c) 15 ˚C.

We measured *D* and its thermal dependence of DOPC-SLB as a control to estimate the effect of fluorocarbon segment of F4-DMPC on the diffusion behavior. DOPC is in the fluid L_α phase as with F4-DMPC at the temperature region in this study, while T_c of non-fluorinated DMPC is 24°C. As we mentioned in the experimental section,α (eq. (3)) of DMPC strongly depends on temperature.[25,29] Therefore DOPC is preferred to DMPC as a control in this study. The MSD-τ plots of all trajectories used for the calculation of ⟨MSD⟩ of DOPC-SLB at each temperature are shown in Figure 6-8, and ⟨MSD⟩-τ plot and *D*-τ plot of DOPC-SLB are shown in Figure 6-9.

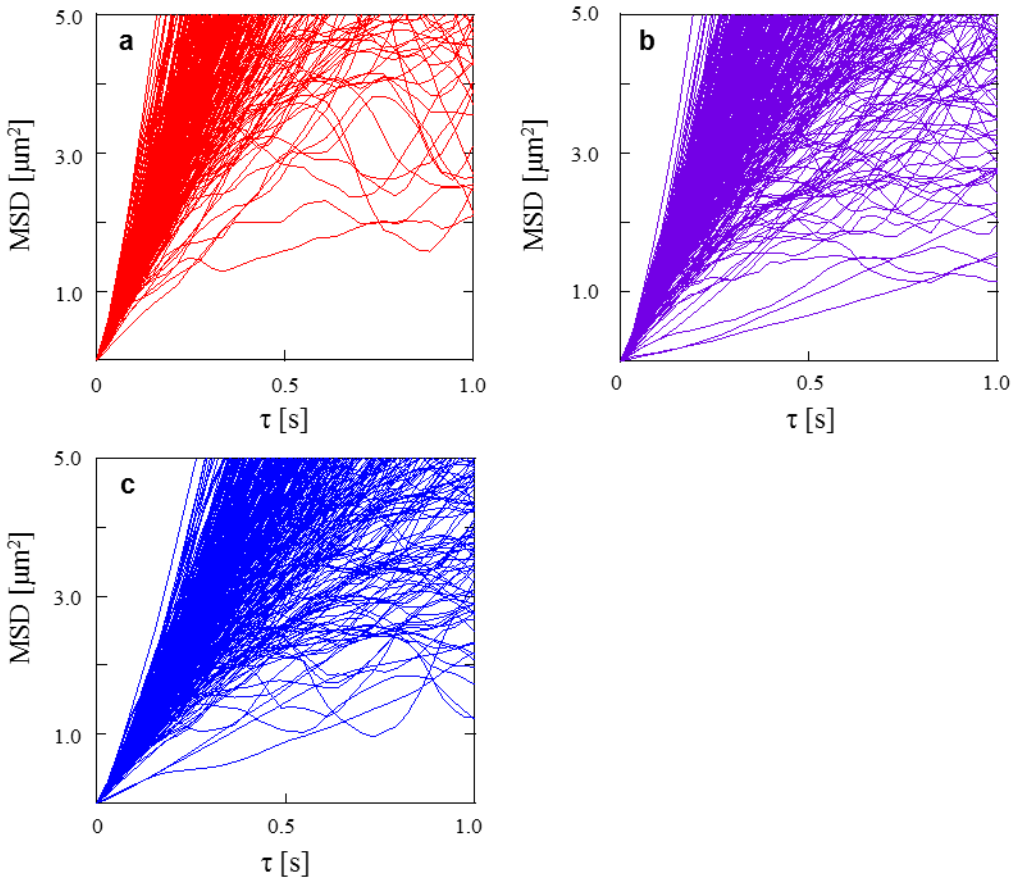

Figure 6-8. MSD versus τ plots of all trajectories obtained for DOPC-SLB at (a) 25 ˚C, (b) 20 ˚C, and (c) 15 ˚C.

We evaluated the apparent activation energy (E'_a) of diffusion from the temperature dependence of D. Figure 6-10 shows the Arrhenius plots obtained from the D of F4-DMPC-SLB and DOPC-SLB at varied temperatures. We obtained E'_a of 39.1 ± 5.3 kJ/mol and 48.2 ± 7.1 kJ/mol for F4-DMPC-SLB and DOPC-SLB from the gradient of each Arrhenius plot (Figure 6-10a and 6-10b, respectively). The values of E'_a estimated in this study are in a reasonable range compared with those reported in the previous FRAP studies, approximately 25 − 45 kJ/mol[33,34] (Table VI-I). We need to evaluate the difference in E'_a obtained in the same experimental condition, because the value of E'_a is also affected by surrounding environments including aqueous solution and substrates (eq. (3)).[22,23] E'_a provides an indication of the intermolecular interaction in SLB, therefore the E'_a values of F4-DMPC and DOPC indicated

that the introduction of a fluorocarbon segment to the hydrophobic parts lead to a weaker intermolecular interaction. It should be noted that in spite of the weaker interaction with surrounding molecules (smaller E'_a) the diffusion was slower (smaller D) in F4-DMPC-SLB than in DOPC-SLB. It indicates the contribution of the A_0 term in eq. (2) overcame the E'_a and T term. Smaller D of F4-DMPC than that of DOPC is because of the steric effect of fluorine which has a larger atomic radius and mass than hydrogen.

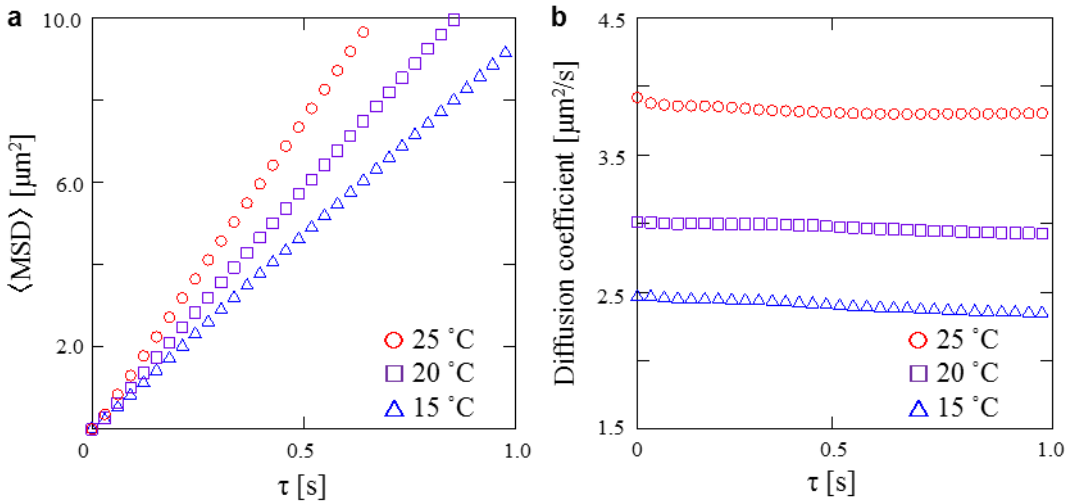

Figure 6-9. (a) ⟨MSD⟩ versus τ plots and (b) diffusion coefficient versus τ plots of DOPC-SLB at 25 ˚C (red circle), 20 ˚C (purple square), and 15 ˚C (blue triangle). Note the difference in the range of the vertical axes from Figure 6-6a. We recorded the trajectories of Rb-DOPE in DOPC-SLB at time resolution of 30.49 ms (33 fps).

The difference in E'_a by 9.1 kJ/mol between F4-DMPC and DOPC is significant, when we refer to the previous studies. E'_a of phospholipids in the L_α phase is rather insensitive to the length or saturation of the hydrocarbon chain, but PCs with unsaturated hydrocarbon tends to show smaller E'_a than those with saturated hydrocarbon,[33,34,48] by approximately 3 − 5 kJ/mol in the previous FRAP studies (Table VI-I). The apparent activation energy E'_a is affected by α as well as E_a (eq. (3)). We calculated the α of F4-DMPC-SLB to be1.4×10^{-3} K^{-1} from Figure 6-3 as described above. If we assume that the α of DOPC-SLB is similar to that of DOPC-GUV

(1.3×10^{-3} K^{-1})[38] or multilamellar vesicles of monounsaturated PCs (2.2×10^{-3} K^{-1})[40], the contribution of the (R/α) term in eq. (3) is estimated to be −0.5 - 2.2 kJ/mol. Therefore the difference in E'_a between the F4-DMPC and DOPC was dominated by the molecular interaction, rather than the area thermal expansion term. As a result of the introduction of a fluorocarbon segment, F4-DMPC had ~10 - 7 kJ/mol weaker molecular interaction in the hydrophobic core than unsaturated DOPC.

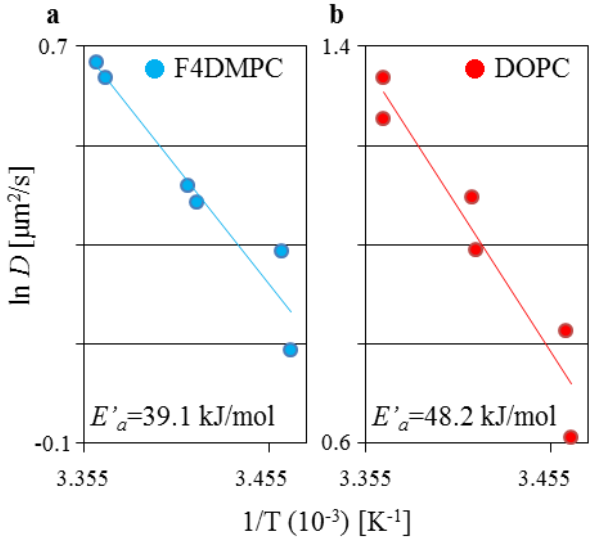

Figure 6-10. Arrhenius plots of diffusion in (a) F4-DMPC-SLB and (b) DOPC-SLB.

It is well known that cholesterol changes the viscoelastic property of lipid membranes. Cholesterol tends to decrease E'_a in a lipid bilayer of saturated acyl chains,[37] and tends to increase E'_a in that of unsaturated chains[49] by approximately 1 − 3 kJ/mol at the molar ratio of phospholipid:cholesterol of 10:2 − 10:5. Addition of other amphiphilic molecules like alcohol also affects the physical properties of the lipid bilayer. Inclusion of butanol and octanol into DPPC bilayer at a molar ratio of lipid:alchol is 1:2 increases the activation energy 6.8 kJ/mol and 10.3 kJ/mol, respectively.[50] The difference in E'_a between the F4-DMPC and DOPC shown in this study achieved the qualitative comparison and the evaluation of the fluorination effect on

the intermolecular interaction in the lipid bilayer.

Table VI-I. Apparent activation energies of non-fluorinated phosphatidylcholines from previous FRAP studies. All lipid bilayers are in L_α phase in these temperature ranges.

Lipid	E'_a [kJ/mol]	Temperature range	Ref
DOPC	40.9	10-40 ˚C	31
DMPC	43.7	28-42 ˚C	31
POPC	28	15-45 ˚C	29
DLPC	30	15-45 ˚C	29
DMPC	33	25-51 ˚C	29
DPPC	26	43-62 ˚C*	29

*The temperature range is different from other lipids because of higher transition temperature of DPPC (T_c = 41 ˚C).

Recently Hasegawa and co-workers proposed the stratified dipole-arrays (DAS) model to explain the aggregation property of perfluoroalkyl compounds.[17] The packing density of partially fluorinated myristic acid $CF_3(CF_2)_n$−$(CH_2)_{12-n}$−COOH in a Langmuir monolayer increased when the length of the fluorocarbon segment (-$(CF_2)_nCF_3$) was n = 7 or longer, by the dipole-dipole interaction due to its helical structure. The dipoles in the perfluoroalkyl chain of n = 3, which corresponds to the hydrophobic tails of F4-DMPC, does not show the dipole-induced packing effect. In the case of F4-DMPC-SLB, the addition of a bulky fluorine atom to the hydrocarbon chains hinders the non-fluorinated hydrocarbon part from taking the well-packed all-trans conformation, meanwhile the fluorinated length is too short for the packing through the dipole-dipole interaction among the fluorinated parts by themselves. These models reasonably explain the low T_c and the unsaturated-PC-like behavior in α of F4-DMPC compared with non-fluorinated DMPC. The absence of the ordered dipole array effect and loose packing due to the steric effect of the fluorocarbon segment result in the attenuation of the intermolecular interaction in the hydrophobic region of the bilayer.

6-4. Summary

We evaluated the intermolecular interaction of F4-DMPC at the hydrophobic core of the bilayer membrane. The temperature dependence of θ and D of F4-DMPC-SLB showed that α of F4-DMPC was not largely different from the values of non-fluorinated PC, but was almost independent of temperature even near the gel-L_α phase transition temperature. The F4-DMPC-SLB had smaller E'_a of diffusion than DOPC by 9.1 kJ/mol. This value was significant compared to the effect of the acyl group species among other non-fluorinated PC, and of the addition of small molecules such as cholesterol and alcohol. The intensity of intermolecular interaction in the hydrophobic core of partially fluorinated lipid bilayer is affected by the competition of the dipole-induced packing effect and the steric effect of the fluorocarbon segment, and our present study is valuable for the quantitative evaluation of the effect of the partial fluorination of the acyl chains.

Reference

1) D. Lingwood and K. Simons, Science **327**, 46 (2010).

2) A. Hirano-Iwata, M. Niwano, and M. Sugawara, TrAC Trends Anal. Chem. **27**, 512 (2008).

3) M. Ø. Jensen and O. G. Mouritsen, Biochim. Biophys. Acta **1666**, 205 (2004).

4) A. G. Lee, Biochim. Biophys. Acta **1666**, 62 (2004).

5) M. G. Gutierrez, K. S. Mansfield, and N. Malmstadt, Biophys. J. **110**, 2486 (2016).

6) M. Bogdanov and W. Dowhan, EMBO J. **17**, 5255 (1998).

7) S. Pal, H. Chakraborty, S. Bandari, G. Yahioglu, K. Suhling, and A. Chattopadhyay, Chem. Phys. Lipids **196**, 69 (2016).

8) M. Sonoyama, T. Kikukawa, Y. Yokoyama, M. Demura, N. Kamo, and S. Mitaku, Chem. Lett. **38**, 1134 (2009).

9) M. P. Krafft and J. G. Riess, Chem. Rev. **109**, 1714 (2009).

10) J.-L. Popot, Annu. Rev. Biochem. **79**, 737 (2010).

11) S. Wang, R. Lunn, M. P. Krafft, and R. M. Leblanc, Langmuir **16**, 2882 (2000).

12) E. Frotscher, B. Danielczak, C. Vargas, A. Meister, G. Durand, and S. Keller, Angew. Chemie Int. Ed. **54**, 5069 (2015).

13) C. Gege, M. F. Schneider, G. Schumacher, L. Limozin, U. Rothe, G. Bendas, M. Tanaka, and R. R. Schmidt, ChemPhysChem **5**, 216 (2004).

14) H. Nakahara, S. Lee, M. P. Krafft, and O. Shibata, Langmuir **26**, 18256 (2010).

15) V. H. Dalvi and P. J. Rossky, Proc. Natl. Acad. Sci. **107**, 13603 (2010).

16) V. V. Chaban, B. Verspeek, and H. Khandelia, J. Phys. Chem. Lett. **4**, 1216 (2013).

17) T. Hasegawa, T. Shimoaka, N. Shioya, K. Morita, M. Sonoyama, T. Takagi, and T.

Kanamori, Chempluschem **79**, 1421 (2014).

18) M. Yoshino, H. Takahashi, T. Takagi, T. Baba, K. Morita, H. Amii, T. Kanamori, and M. Sonoyama, Chem. Lett. **41**, 1495 (2012).

19) H. Takahashi, M. Yoshino, T. Takagi, H. Amii, T. Baba, T. Kanamori, and M. Sonoyama, Chem. Phys. Lett. **559**, 107 (2013).

20) M. Yoshino, T. Kikukawa, H. Takahashi, T. Takagi, Y. Yokoyama, H. Amii, T. Baba, T. Kanamori, and M. Sonoyama, J. Phys. Chem. B **117**, 5422 (2013).

21) M. Yoshino, H. Takahashi, T. Takagi, T. Baba, K. Morita, H. Amii, T. Kanamori, and M. Sonoyama, Chem. Lett. **41**, 1495 (2012).

22) P. F. F. Almeida and W. L. C. Vaz, in *Handb. Biol. Phys.*, edited by R. Lipowsky and E. Sackmann (Elsevier, 1995), pp. 305–357.

23) V. Schram and S. B. Hall, Biophys. J. **86**, 3734 (2004).

24) M. D. King and D. Marsh, Biochim. Biophys. Acta - Biomembr. **862**, 231 (1986).

25) D. D. Gross and W. W. Webb, in *Spectrosc. Membr. Probes Vol. II*, edited by L. M. Loew (CRC Press, Boca Raton, FL, 1988), pp. 19–45.

26) G. J. Schütz, H. Schindler, and T. Schmidt, Biophys. J. **73**, 1073 (1997).

27) A. Sergé, N. Bertaux, H. Rigneault, and D. Marguet, Nat. Methods **5**, 687 (2008).

28) R. Metzler, J.-H. Jeon, A. G. Cherstvy, and E. Barkai, Phys. Chem. Chem. Phys. **16**, 24128 (2014).

29) I. F. Sbalzarini and P. Koumoutsakos, J. Struct. Biol. **151**, 182 (2005).

30) R. Tero, Materials **5**, 2658 (2012).

31) D. Keller, N. B. Larsen, I. M. Møller, and O. G. Mouritsen, Phys. Rev. Lett. **94**, 25701 (2005).

32) H. M. Seeger, A. Di Cerbo, A. Alessandrini, and P. Facci, J. Phys. Chem. B **114**, 8926

(2010).

33) W. L. C. Vaz, R. M. Clegg, and D. Hallmann, Biochemistry **24**, 781 (1985).

34) L. K. Tamm and H. M. McConnell, Biophys. J. **47**, 105 (1985).

35) J. F. Nagle and S. Tristram-Nagle, Biochim. Biophys. Acta - Rev. Biomembr. **1469**, 159 (2000).

36) E. Evans and D. Needham, J. Phys. Chem. **91**, 4219 (1987).

37) P. F. F. Almeida, W. L. C. Vaz, and T. E. Thompson, Biochemistry **31**, 6739 (1992).

38) L. Parolini, B. M. Mognetti, J. Kotar, E. Eiser, P. Cicuta, and L. Di Michele, Nat. Commun. **6**, 5948 (2015).

39) J. Pan, S. Tristram-Nagle, N. Kucerka, and J. F. Nagle, Biophys. J. **94**, 117 (2008).

40) N. Kučerka, M.-P. Nieh, and J. Katsaras, Biochim. Biophys. Acta - Biomembr. **1808**, 2761 (2011).

41) J. Pencer, M.-P. Nieh, T. A. Harroun, S. Krueger, C. Adams, and J. Katsaras, Biochim. Biophys. Acta - Biomembr. **1720**, 84 (2005).

42) N. Chu, N. Kučerka, Y. Liu, S. Tristram-Nagle, and J. F. Nagle, Phys. Rev. E **71**, 41904 (2005).

43) M. Saxton, Biophys. J. **70**, 1250 (1996).

44) R. Tero, G. Sazaki, T. Ujihara, and T. Urisu, Langmuir **27**, 9662 (2011).

45) A. Berquand, P. Mazeran, J. Pantigny, V. Proux-Delrouyre, J. Laval, and C. Bourdillon, Langmuir **19**, 1700 (2003).

46) E. I. Goksu, B. A. Nellis, W.-C. Lin, J. H. Satcher, J. T. Groves, S. H. Risbud, and M. L. Longo, Langmuir **25**, 3713 (2009).

47) F. Okada and K. Morigaki, RSC Adv. **5**, 1507 (2015).

48) Y. Wu, M. Stefl, A. Olzyńska, M. Hof, G. Yahioglu, P. Yip, D. R. Casey, O. Ces, J.

Humpolíčková, and M. K. Kuimova, Phys. Chem. Chem. Phys. **15**, 14986 (2013).

49) N. Bag, D. H. X. Yap, and T. Wohland, Biochim. Biophys. Acta - Biomembr. **1838**, 802 (2014).

50) S. Rifici, C. Corsaro, C. Crupi, V. C. Nibali, C. Branca, G. D'Angelo, and U. Wanderlingh, J. Phys. Chem. B **118**, 9349 (2014).

Chapter 7

Conclusion

Chapter 7. Conclusion

In the doctoral course, I have constructed new artificial lipid bilayer systems on the basis of supported lipid bilayers (SLBs). I fabricated SLBs on graphene oxide (GO) deposited on a SiO_2/Si substrate, for the development of a new method to measure the behavior of biomolecules in lipid bilayers applying the quenching function of GO. As another subject, I investigated the physicochemical properties of the bilayer of a synthetic partially fluorinated phospholipid in the SLB system.

In Chapter 3, I investigated the SLB formation process on GO. I prepared SLB of 1,2-dioleoyl-sn-glycero-3-phosphocoholine (DOPC) on GO deposited on a thermally oxidized SiO_2/Si substrate by the vesicle fusion method, and evaluated its membrane structure and membrane fluidity by using an atomic force microscope (AFM) and a fluorescence microscope. AFM topography and FRAP measurement indicated that fluid and planar lipid bilayers were formed on GO after the incubation of GO/SiO_2/Si substrate in $CaCl_2$-containing DOPC vesicle suspension. From the AFM observation, I found that not only single lipid bilayer, similar to the SLB formation on inorganic substrates, but also double lipid bilayers were formed on GO. I proposed a structural model of the GO/SLB system. I established a protocol for the formation of SLB on GO, and this GO/SLB system is the fundamental platform for the measurement of biomolecules in the plasma membrane model using the functions of GO.

In Chapter 4, I investigated the modification of the SLB surface using Qdot as a fluorescence probe to evaluate the membrane fluidity of SLB/GO systems quantitatively. I conjugated Qdots, which are premodified with a hetero-cross-linker and 2-(2-aminoethoxy) ethanol to the SLB

surface. I performed single particle tracking (SPT) for the measurement of diffusion coefficient (*D*) of DOPC-SLB formed on GO. To suppress the nonspecific adsorption of Qdot to the SLB surface, I used DOPC-SLB containing 5% 1,2-distearoyl-sn-glycero-3-phospho-ethanolamine-N-[amino(polyethylene glycol)-2000] (PEG-DSPE). Diffusion of Qdot-conjugated lipids was observed in the SLB formed on GO and SiO_2, and I obtained sufficiently long trajectories of single Qdot-conjugated lipids for reliable analysis of mean-square displacement. The D-τ plot showed that the diffusion behavior of the Qdot-conjugated lipid was normal random diffusion even in the SLB on GO. In addition, I found that the lipid diffusion was slower in the SLB on GO than that on SiO_2 by comparing D of a single Qdot-conjugated lipid diffusing between the GO and SiO_2 regions. I revealed the difference in the membrane fluidity between SLBs on GO and the SiO_2/Si substrate by the SPT method using Qdot as a fluorescence probe.

In Chapter 5, I evaluated the fluorescence quenching efficiency by GO and the diffusion behavior of lipids in SLB on GO by the SPT measurement using Qdots as a fluorescence probe. I obtained sufficiently long trajectories of single Qdot-conjugated lipids for reliable analysis of mean-square displacement, and evaluated the quenching efficiency from the fluorescence intensity measured simultaneously with the trajectory. Furthermore, I estimated the Qdot-GO distance from the quenching efficiency based on fluorescence resonance energy transfer (FRET) theory for two-dimensional quencher. The estimated distances between Qdot and GO were distributed to ~10 nm and more than 17 nm. These were reasonable values when Qdot is conjugated to the outermost surface of single and double SLB as the SLB/GO structural model proposed in Chapter 3. AFM topographies of SLB containing PEG-DSPE on GO and on bare SiO_2/Si substrate indicated that depression region derived from PEG-DSPE was appeared on

only the GO regions. I clarified that the reason for the decrease in *D* of SLB on GO is due to the localization of PEG-DSPE on GO. These results suggested that the properties and specific structure of the GO surface consisting of nanoscale hydrophilic and hydrophobic domains trapped more rigid lipids in promoted affected the lipid assembly of SLB, resulting in the lateral diffusion of lipids. I revealed that the quenching efficiency of GO in SLB/GO systems and the effect of concentrating rigid lipid domain on GO. This concentration effect of specific lipid domains on GO shows that the possibility to control the formation of lipid rafts on GO.

In Chapter 6, I investigated the intermolecular interaction of 1,2-di-(11,11,12,12,13,13, 14,14,14-nonafluorotetradecanoyl)-sn-glycero-3-phosphocholine (F4-DMPC) at the hydrophobic core of the bilayer membrane. The temperature dependence of area fraction (θ) of F4-DMPC-SLB showed that the area thermal expansion coefficient (α) of F4-DMPC was not largely different from the values of non-fluorinated PC, but was almost independent of temperature even near the gel-L_α phase transition temperature. The F4-DMPC-SLB had smaller appearance activation energy E'_a of diffusion than DOPC by 9.1 kJ/mol. This value was significant compared to the effect of the acyl group species among other non-fluorinated PC, and of the addition of small molecules such as cholesterol and alcohol. The intensity of intermolecular interaction in the hydrophobic core of partially fluorinated lipid bilayer is affected by the competition of the dipole-induced packing effect and the steric effect of the fluorocarbon segment. This study is valuable for the quantitative evaluation of the effect of the partial fluorination of the acyl chains in bilayer system.

In these work, I have established the fabrication protocol of SLB on GO, and have evaluated the physicochemical properties of SLB/GO systems. I revealed that the SLB/GO system is

formed by different process from a generally used hydrophilic substrate in the vesicle fusion method. And I found that a specific lipid domain were localized on GO. Moreover, I demonstrated that fluorescence intensity of fluorescence probe in SLB/GO system varies depending the on the distance from GO. I expect that a new measurement method using the SLB/GO system will enables us measure the Z-position of biomolecules in lipid bilayer, in addition to the traditionally measurement of molecular diffusion on the X-Y plane. The moderate interaction of the fluorinated lipid will be useful when one introduce membrane proteins in to an artificial bilayer system keeping their active functions and structure. I expect that the fabrication of new artificial lipid bilayer systems applying GO and fluorinated lipids lead to developments of tools for elucidating behavior of biomolecules such as membrane reactions and glycolipids in lipid bilayer.

List of publications and presentations

Publications

1. Yoshiaki OKAMOTO, Kazuyuki TSUZUKI, Seiji IWASA, Ryosuke ISHIKAWA, Adarsh SANDHU, and Ryugo TERO, “Fabrication of Supported Lipid Bilayer on Graphene Oxide”, *Journal of Physics: Conference Series*, **352**, 012017 (1-6), 2012 (peer reviewed).

2. Yoshiaki OKAMOTO, Toshinori MOTEGI, Kohei MORITA, Toshinori TAKAGI, Hideki AMII, Toshinori KANAMORI, Masashi SONOYAMA, and Ryugo TERO, “Lateral Diffusion and Molecular Interaction in a Bilayer Membrane Consisting of Partially Fluorinated Phospholipid”, *Langmuir* **32**, pp 10712-10718, 2016 (peer reviewed).

3. Yoshiaki OKAMOTO, Toshinori MOTEGI, Seiji IWASA, Adarsh SANDHU, and Ryugo TERO, “Fluidity evaluation of cell membrane model formed on graphene oxide with single particle tracking using quantum dot”, *Japanese Journal of Applied Physics* **54**, 04DL09 (1-6), 2015 (peer reviewed).

Presentations

-International conferences

1. Y. Okamoto, K. Tsuzuki, S. Iwasa, R. Ishikawa, A. Sandhu and R. Tero

"Fabrication of Supported Lipid Bilayer on Graphene Oxide", The Asia-Pacific Interdisciplinary Research Conference (AP-IRC) 2011, Nov 18, 2011, Toyohashi, Japan, (Poster).

2. Y. Okamoto, K. Tsuzuki, Y. Okamoto, S. Iwasa, R. Ishikawa, A. Sandhu and R. Tero

"Fabrication and Structural Observation of Graphene-Oxide-Supported Lipid Bilayer", 12th Australia- Japan Colloid and Interface Science Symposium, Nov 21, 2011, Cairns, Australia, (Poster).

3. Y. Okamoto, K. Tsuzuki, S. Iwasa, R. Ishikawa, A. Sandhu and R. Tero

"Fabrication of supported lipid bilayers on full-coverage graphene oxide for single molecule observation", International Association of Colloid and Interface Scientists, Conference (IACIS 2012), May 15, 2012, Sendai, Japan, (Poster).

4. Y. Okamoto, K. Tsuzuki, S. Iwasa, R. Ishikawa, A. Sandhu and R. Tero

"Graphene oxide-supported lipid bilayer platform as a cell membrane model", 2012 International Conference on Flexible and Printed Electronics (ICFPE2012), Sep 07, 2012, Tokyo, Japan, (Poster).

5. Y. Okamoto, S. Iwasa, A. Sandhu and R. Tero

"Formation of lipid bilayers on graphene oxide and single molecule observation", The Irago Conference: The Asia-Pacific Interdisciplinary Research Conference (AP-IRC 2012), Nov 15,

2011, Tahara, Japan, (Poster).

6. Y. Okamoto, S. Iwasa, A. Sandhu and R. Tero

"Single molecule observation of lipid bilayers on graphene oxide", 7th International Conference on Molecular Electronics and Bioelectronics (M&BE7), Mar 19, 2013, Fukuoka, Japan, (Poster).

7. Y. Okamoto, T. Motegi, S. Iwasa, A. Sandhu and R. Tero

"Quantum Dot Conjugation to Model Cell Membranes on Graphene Oxide for the Evaluation of Membrane Fluidity", The Irago Conference 2013, Oct 25, 2013, Tahara, Japan, (Poster).

8. Y. Okamoto, T. Motegi, S. Iwasa, A. Sandhu and R. Tero

"Quantum dots conjugation to supported lipid bilayers formed on graphene oxide", 12th International Conference on Atomically Controlled Surfaces, Interfaces and Nanostructures (ACSIN-12), Oct 25, 2013, Tsukuba, Japan, (Poster).

9. Y. Okamoto, T. Motegi, S. Iwasa, A. Sandhu and R. Tero

"Fluidity Evaluation of Cell Membrane Model Formed on Graphene Oxide with Single Particle Tracking Using Qdot", International Conference on Solid State Devices and Materials (SSDM2014), Sep 10, 2014, Tsukuba, Japan, (Poster (with flash talk)).

10. Y. Okamoto, T. Motegi, S. Iwasa, A. Sandhu and R. Tero

"Single particle tracking of Qdot-conjugated lipid bilayer on graphene oxide for evaluation of membrane fluidity", The 7th International Symposium on Surface Science (ISSS-7), Nov 03,

2014, Matsue, Japan, (Poster).

11. Y. Okamoto, T. Motegi, M. Kohei, T. Takagi, T. Kanamori, M. Sonoyama and R. Tero "Physicochemical Property of Partially Fluorinated Phospholipid in Supported Lipid Bilayer", iCeMS International Symposium: Hierarchical Dynamics in Soft Materials and Biological Matter, Sep 25, 2015, Kyoto, Japan, (Poster (with flash talk)).

12. Y. Okamoto, T. Motegi, S. Iwasa, A. Sandhu and R. Tero "Fluidity evaluation of supported lipid bilayer prepared on graphene oxide based on single particle tracking", The 2015 International Chemical Congress of Pacific Basin Societies (PacifiChem2015), Dec 17, 2015, Hawaii Convention Center, Honolulu, HI, USA, [MTLS1423] (Poster).

13. Y. Okamoto, S. Saito, S. Iwasa and R. Tero "Localization of Microdomains in Multicomponent Lipid Bilayer Membranes on Graphene Oxide", 2016 KJF (Korea-Japan Joint Forum) International Conference on Organic Materials for Electronics and Photonics (KJF-ICOMEP 2016), Sep 5, 2016, Fukuoka, Japan, [PS-145] (Poster).

14. Y. Okamoto, S. Saito, S. Iwasa and R. Tero "Concentration Effect of Graphene Oxide on Microdomains in Multicomponent Lipid Bilayer Membranes", 2016 International Conference on Solid State Devices and Materials (SSDM2016), Sep 28, 2016, Tsukuba, Japan, [PS-11-04] (Poster).

-Domestic presentations (in Japanese)

10 oral presentations and 5 poster presentations.

Awards

1. ICFPE Student Poster Award: "Graphene oxide-supported lipid bilayer platform as a cell membrane model", 2012 International Conference on Flexible and Printed Electronics (ICFPE2012)

2. M&BE7 Outstanding Student Poster Award: "Single molecule observation of lipid bilayers on graphene oxide", 7th International Conference on Molecular Electronics and Bioelectronics (M&BE7)

3. Best Student Poster Award: "Localization of Microdomains in Multicomponent Lipid Bilayer Membranes on Graphene Oxide", 2016 KJF (Korea-Japan Joint Forum) International Conference on Organic Materials for Electronics and Photonics (KJF-ICOMEP 2016)

Acknowledgement

All of my studies in doctor course were carried out under the supervision of Associate Professor Ryugo Tero. I would like to express here the deepest gratitude to him for the opportunity to meet this attractive theme.

I am very much grateful to Professor Seiji Iwasa for invaluable advices and tremendous support. I am also grateful to Associate Professor Kazutaka Shibatomi. His technical comments based on organic chemistry were greatly helps.

I am deeply grateful to Professor Adarsh Sandhu in Department of Electrical and Electronic Information Engineering in

Toyohashi University of Technology (currently in University of Electro-Communications) and Dr. Ryosuke Ishikawa in Tokyo Institute of Technology (currently Assistant Professor in Niigata University) for advices on the preparation of graphene oxide.

I would like to thank Dr. Toshinori Motegi (currently Assistant Professor in Gunma University) for technical support and expertise on single particle tracking. I appreciate the kind support on the preparation of SiO2/Si substrate from Dr. Hirokazu Nakazawa and Professor Kazuaki Sawada.

I would like to the deep appreciation to Professor Masashi Sonoyama in Gunma University for insightful comments and fruitful discussions on the study of fluorinated lipids described in Chapter 6. I am also grateful to Mister Toshiyuki Takagi in National Institute of Advanced Industrial Science and Technology and Kohei Morita in Gunma University for providing their synthesized F4DMPC.

All of my studies in doctor course were supported by Japan Society for the Promotion of Science. I am grateful for the tremendous economic support over three years.

Earnest thanks go to all students of Tero laboratory and all collaborators for great deal of support and collaborations.

At last, I am heartfelt thanks to my family for long-term support and considerable encouragement.